AD701 788

FINAL REPORT

"Study of Various Aspects of Raman Scattering Using Gas Lasers"

Period Covered: Aug. 1, 1965 - July 31, 1968

Under Supervision of:
Project Scientist: Professor A. Javan
Telephone: 868-4860, Ext. 5088

Contract Nonr 3963(22) Modification 1, 2
Project #NR 014-209/7-17-67 (Code 421)
DSR #74979

Massachusetts Institute of Technology
Cambridge, Massachusetts 02139

TITLE

Study of Various Aspects of Raman Scattering Using Gas Lasers

FINAL REPORT

Period Covered: August 1, 1965 to July 31, 1968

under supervision of

Project Scientist: Professor A. Javan
Telephone: Un 4-6900 Ext. 5088

under

Contract Nonr 3963(22) Modification #1 and 2
Project # NR 014-209/7-17-67 (Code 421)

Arpa Authorization Order # 306

Starting Date: August 1, 1965 Expiration Date: July 31, 1968

Amount of Contract $120,340

MIT Project # DSR 74979

This research is part of Project DEFENDER under the joint sponsorship of the Advanced Research Projects Agency, the Office of Naval Research, and the Department of Defense.

Issue Date: January 30, 1969

Laser-Induced Line Narrowing Effect in Coupled Doppler-Broadened Transitions

M. S. Feld and A. Javan

ABSTRACT

The line shape of a Doppler-broadened transition is dramatically altered by the presence of a laser field resonating with a second Doppler-broadened transition sharing a common level: two narrow resonances of different widths appear superimposed upon the broad background signal at frequencies symmetrically located about the corresponding line center. The effect has already found application in a number of seemingly different though intimately related studies, including high resolution h. f. s. and isotope shift determinations. The theory of the effect is developed with reference to these applications. The treatment is formulated in terms of transition rates induced by two classical fields resonantly interacting with a pair of coupled Doppler-broadened transitions of arbitrary frequencies. The perturbation approach adopted is valid for one field fully saturating its transition; the resulting line shape expression exhibits important power broadening effects. This approach is equivalent to the familiar density matrix formulation, which is also presented. Various features of the resulting expression are discussed in detail as they apply to two precision spectroscopic applications, Mode Crossing and Spontaneous Emission Line Narrowing. The connection with previous work is also discussed.

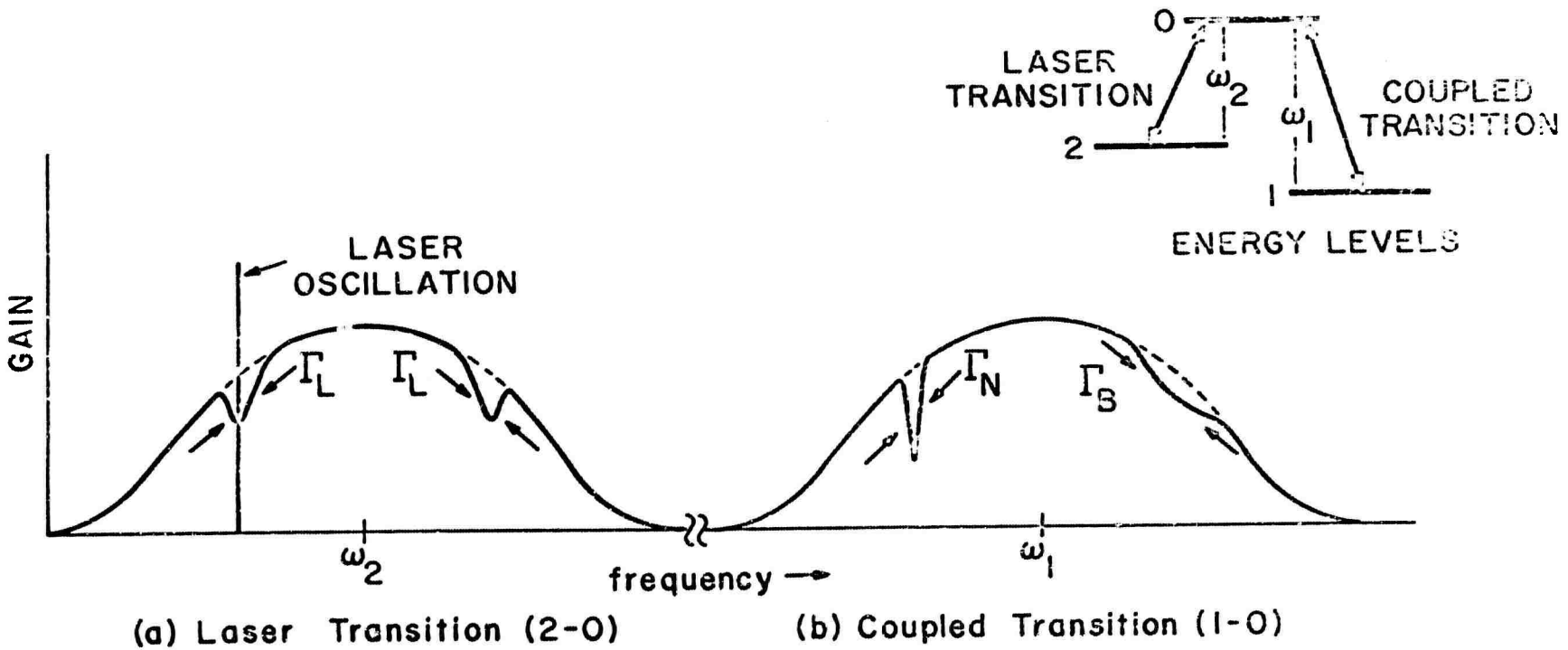

FIGURE 1: Spectrum Of Line Narrowing Induced In The Doppler Gain (Or Attenuation) Profiles Of (a) Laser And (b) Coupled Transitions

I. INTRODUCTION

It is well known[1] that the overall gain profile of a Doppler-broadened laser transition is dramatically influenced by the presence of the laser field. This may be demonstrated by scanning the gain profile with a weak, monochromatic probe field colinear with the laser field: As the probe field is tuned through the transition, two identical sharp decreases in gain appear superimposed upon the broad lineshape, one at the laser frequency and one symmetrically located on the opposite side of the atomic line center. [Fig. 1(a)]. These resonant decreases occur because the standing-wave field within the laser cavity selectively interacts with atoms whose velocities Doppler-shift one of its travelling-wave components into resonance. This produces changes in the laser level populations -- an increase in the lower level population and a decrease in the upper level population -- over two intervals symmetrically located about the center of the velocity distribution. These changes reflect themselves in depletions in the gain profile over the corresponding frequency intervals. The extent of these intervals is determined by the natural widths (or, more generally, the homogeneous widths) of the atomic transitions.

In the foregoing discussion it is assumed that the laser field is detuned from ω_2, the atomic center frequency. As its frequency approaches within a natural width of ω_2, the two resonant decreases merge into a single one. However, let us primarily consider those cases in which the laser frequency is detuned and the change signals are well resolved.

The line shape of a second Doppler-broadened transition formed by either of the levels of the laser transition and a third level is also considerably altered by laser oscillation: Scanning as before the gain (or attenuation) profile of this transition with a weak probe field, one again finds two sharp resonances at frequencies symmetrically located about the corresponding line center. These change signals differ from those of the laser transition in one remarkable aspect: one can be considerably narrower than the other. [Fig. 1 (b)]. We shall refer to the widths of the broad and narrow change signals as Γ_B and Γ_N, respectively. For example, if the center frequency of the coupled transition (0 - 1) is close to that of the laser transition (0 - 2) then, for a weakly-saturating laser field, $\Gamma_N = \gamma_1 + \gamma_2$ and $\Gamma_B = \gamma_1 + \gamma_2 + 2\gamma_0$, with γ_j the decay rate of level j. In comparison, the change signals of the laser transition are each of width $\Gamma_L = \gamma_0 + \gamma_2$.

Similar lineshape features would be observed in the closely related situation in which the fluorescence from either of the laser levels to a third level is monitored along the laser axis. Note that the resulting spontaneous emission spectrum directly follows the spectrum of emission stimulated by a weak probe field tuned through the coupled transition when the lower level population of the coupled transition is ignored. As an illustration, suppose the laser field were tuned to the low frequency side of its Doppler profile: For emission originating in its upper level, the laser-induced change signals would appear as resonant decreases of widths Γ_N below ω_1 and Γ_B above ω_1, with ω_1 the

fluorescence center frequency. In contrast, emission originating in the lower laser level would result in resonant increases with the positions of the broad and narrow change signals interchanged. A further noteworthy distinction is the differing radiative origins of the change signals: in the former case they result primarily from double-quantum transitions, while in the latter case they are primarily due to single-quantum transitions. This important distinction is elaborated below.

Since Γ_N and Γ_B are generally much narrower than the Doppler widths we shall refer to this effect as "Laser-Induced Doppler Line Narrowing".

As has been noted, the stimulated and spontaneous versions of Laser-Induced Doppler Line Narrowing are different manifestations of the same basic quantum-mechanical effect. Nevertheless, important applications of these versions bear little resemblance to one another on the surface. A major purpose of this paper is to relate the basic effect to these intimately connected though seemingly different applications. In some of these $\Gamma_B >> \Gamma_N$, causing the differing width characteristics to reveal themselves in particularly striking ways.

Several pulbications dealing with details of the line shape in various special cases have appeared previously.[2-8] The initial presentation[2] by Schlossberg and Javan, a quantum-mechanical analysis of the third-order polarization induced by two classical fields, demonstrated the applicability of the narrow resonance Γ_N to high-resolution studies of closely-spaced

Doppler-broadened laser transitions [Fig. 2(b)]. The latter treatment also applies to a cascade system [Fig. 2(c)] in which the middle level lies about halfway between the upper and lower levels. Subsequently, Notkin, Rautian and Feoktistov presented a quantized field calculation[4] which described the spontaneous emission spectrum arising from one of the levels of a weakly-saturated laser transition. A recent discussion[5] by Holt, formulated on the basis of two-photon transitions induced by the laser field, analyzed the frequency profile of the spontaneous emission arising from the lower laser level [Fig. 2(c)]. This treatment neglects single-quantum events and would not apply, for example, to the case of spontaneous emission arising from the upper laser level. The treatment of Ref. 4, however, is valid in either case. A subsequent letter[7] by the present authors analyzed the spontaneous and stimulated versions of Laser-Induced Doppler Line Narrowing experiments by means of a classical field approach, emphasizing their close relationship; the theoretical treatment took into account the influence of both single-quantum and double-quantum transitions, and included, in addition, intensity-dependent line broadening effects.[9]

The present paper is, in part, an elaboration of that letter,[7] and contains additional detailed discussions. The treatment is formulated in terms of transition rates induced by two classical fields resonantly interacting with a pair of coupled Doppler-broadened transitions of arbitrary frequencies. The method of analysis is an extension of the one[10] adopted some time ago in calculating the line shape details of a three level maser.

In this approach two distinct processes emerge: the first, a double-quantum transition, involves the exchange of a photon with each of the two applied fields; the second, an inherently single-quantum act, includes the influence of one field on the rate at which single-quantum transitions are induced by the other field. This distinction is not apparent in the usual density-matrix formalism in which the induced polarization is calculated. The two approaches are, of course, equivalent; their connection will be clarified below. Moreover, the theoretical approach adopted is not restricted to a third-order polarization calculation, and is valid for one field fully saturating its transition; the resulting line shape expression exhibits important power broadening effects. We are able to obtain such an expression because in the applications discussed here it is generally sufficient to consider the standing-wave laser field to be detuned from the center of its Doppler-broadened gain profile. Then its travelling-wave components do not couple to each other and, consequently, may be treated independently. Furthermore, major applications and their important physical features are adequately described by considering the weak field gain of one transition as influenced by a fully-saturated coupled transition; the approach may be readily extended, if necessary, to include higher order effects.

The approach of Notkin, Rautian and Feoktistov,[4] which calculates the laser-induced spontaneous emission spectrum, is complementary to ours. That treatment is formulated considering both radiation fields in quantized form. The actual calculation is somewhat simplified, however, by considering the laser field in its classical form, a procedure, of course,

justifiable for radiation oscillators in states of high excitation. The spontaneous emission field, however, is kept in its quantized form. The introduction of field quanta leads naturally to a mathematical development considerably different from our classical field approach. The computations are rather involved, and relevant results are obtained only for a weakly-saturating laser field. As discussed below, the latter results agree with the weak-saturation limit of those obtained here. In the discussions of Ref. 4 the connection with experimental observations[11, 12] and theory[2] of an earlier stimulated version of the effect has not been made. This connection, which is not apparent on the surface, is clarified below.

The calculation of the Doppler-broadened response is carried out in Part II. Section IIA considers the interaction of two monochromatic classical travelling-wave fields with a group of three level atoms moving with fixed velocity. One field is assumed to fully saturate the transition with which it resonates; the second field, assumed weak, probes the coupled transition. The emitted power at the probe frequency is calculated in terms of transition rates, as indicated above. The subsequent average over atomic velocities, which leads to the Doppler-broadened travelling-wave response, is outlined in Section IIB, together with a discussion of the resulting line shape. The extension of the travelling-wave analysis to standing-wave applications is presented in Section IIC, which also discusses the specifically

standing-wave effects arising when the intense field is tuned to its atomic center frequency. Wherever possible, the presentation of detailed algebraic manipulations and proofs has been deferred to Appendices.

Part III discusses, by example, important features of Laser-induced Doppler Line Narrowing. Section IIIA examines the frequency dependence of the atomic response prior to Doppler averaging. Section IIIB continues by discussing the extension of the line narrowing effect to the spontaneous-emission version mentioned above, explaining the connection with earlier formulations. In Sections IIIC and IIID two important applications are examined in detail: The first,[11] a technique involving two classical fields, enables structure of Doppler-broadened systems with closely spaced levels to be measured with great accuracy. This technique has already been employed in measuring hyperfine structure[12] and paramagnetic properties[13] of several excited atomic levels. The second,[14] based upon the spontaneous emission version, has been utilized in isotope shift[15] and linewidth paramete[16,17] measurements in Ne.

The results of this paper are also directly applicable to the extraordinary behavior of atomic Oxygen fine-structure laser oscillations at 8446 Å,[18] already briefly discussed in Refs. 3, 7 and 19. In that case other physical processes, entirely unrelated to the present discussions, are of great importance. We prefer to discuss these together in a separate publication[20] which will utilize expressions derived below.

II. DOPPLER-BROADENED GAIN

We now proceed to calculate the interaction of a weak, monochromatic probe field with one of the transitions of a Doppler-broadened three level system, as influenced by a saturating field resonating with the coupled transition. In order to describe applications within a Fabry-Perot cavity one must consider the possibility of fields in the form of standing waves, as well as travelling waves. For reasons given below, the major features of important standing-wave applications may be understood by analyzing the case in which the intense field is detuned from the center of its broad Doppler profile. Considerable simplification then results, and the standing-wave response may be analyzed in terms of pairs of travelling-wave fields interacting with the respective transitions of the three level system. As will become evident, the relative propagation direction of probe and saturating field components is of crucial importance: fields propagating in the same direction lead to a probe-field line shape which is strikingly different from that due to oppositely-propagating fields.

The atoms of a Doppler-broadened gas may traverse many wavelengths of the applied fields before decaying. We adopt here the simple picture of atomic motion in which an atom produced in a particular state travels undeflected with constant velocity as it decays. The calculation of induced emission may be divided into two stages: The response is first obtained for a band of three level atoms within a narrow range of axial

velocities interacting with the applied travelling-wave fields; this quantity is then summed over the entire distribution of velocities, thus obtaining the complete emission profile. The first stage, the calculation of the ensemble-averaged travelling-wave response, may be carried out in several ways. The induced dipole moment of an atom produced in a given state may be calculated from the Schrödinger equation. Equivalently, one may calculate the rate at which an atom produced in a given state makes transitions to other states. In either case the response of the entire velocity ensemble is obtained by averaging the quantity calculated over all initial conditions. The transition rate approach, which has the important advantage of identifying the various radiative processes by which an atom emits and absorbs photons, is presented in Section IIA. The connection between transition rates and induced dipole moments is examined in Appendix B. An alternate derivation of the line shape using the ensemble-averaged density matrix equations of motion, and related discussions, are presented in Appendix C.

A. Ensemble-Averaged Response: Transition Rate Approach

The resonant interaction of two monochromatic fields, E_1 and E_2, with a three level system was treated in Ref. 10 for cases where Doppler broadening is negligible (e.g., the microwave region) and the decay rates, considered equal for all three levels, were assumed to result from hard collisions. The perturbation method consisted of first obtaining a closed-form solution to the Schrodinger equation for $E_1 = 0$ and E_2 arbitrary, and then using this result to generate a solution valid to first order in E_1. The

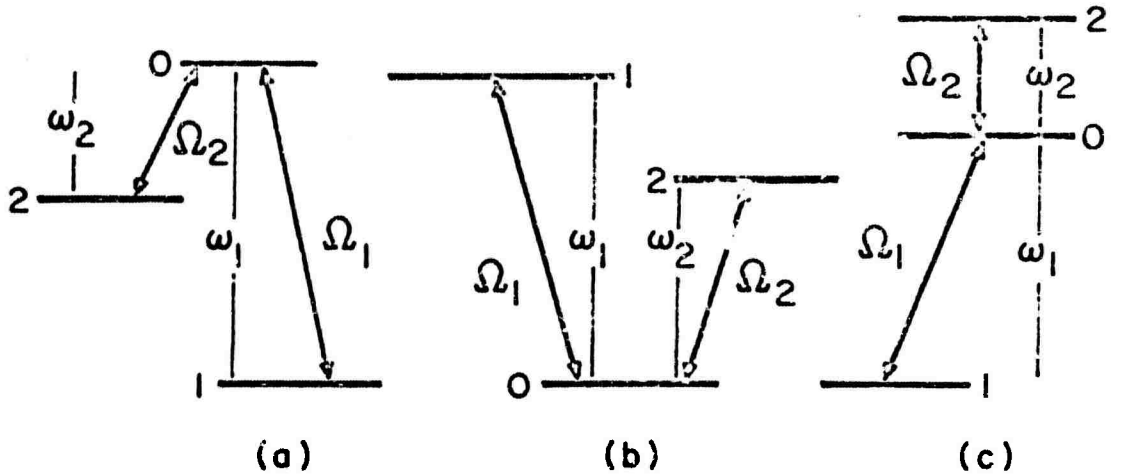

FIGURE 2: Energy Level Configurations

present section is, in part, a generalization of that method valid for levels with differing decay rates.

The three level systems to be studied are of the type shown in Fig. 2(a), (b), (c). Level 0, the common level, is coupled to levels 1 and 2 by electric dipole matrix elements μ_{10} and μ_{20}, respectively. Denote the energy of level j by $\hbar W_j$, and let $|W_j - W_0| = \omega_j$; ω_1 and ω_2 fall in the optical-infrared region we shall assume $(\omega_1 - \omega_2)$ is large compared to the natural linewidths. In the present Section we consider the "inverted-V" level configuration, in which level 0 lies highest [Fig. 2(a)]. The treatment is easily extended to cases in which level 0 lies below either or both of levels 1 and 2. This extension is discussed in Appendix C.

The system interacts with a strongly saturating field $E_2(z, t;\epsilon)$ at Ω_2, a frequency close to ω_2. The resonance at ω_1 is probed by the weak field $E_1(z, t)$ at variable frequency Ω_1. To allow for both possible relative propagation directions, $E_1(z, t)$ is taken to be travelling in the positive $(+z)$ direction, while $E_2(z, t;\epsilon)$ may propagate in either positive $(\epsilon = +1)$ or negative $(\epsilon = -1)$ directions. Specifically,

$$E_1(z, t) = E_1^o \cos(\Omega_1 t - k_1 z + \phi_1) = A_1(z) e^{i\Omega_1 t} + \text{c. c.}$$

and (1 a)

$$E_2(z, t;\epsilon) = E_2^o \cos(\Omega_2 t - \epsilon k_2 z + \phi_2) = A_2(z;\epsilon) e^{i\Omega_2 t} + \text{c. c.},$$

with $k_j = \Omega_j / c$; thus

$$A_1(z) = \frac{1}{2} E_1^o e^{i\phi_1 - ik_1 z}$$

and (1 b)

$$A_2(z;\epsilon) = \frac{1}{2} E_2^o e^{i\phi_2 - i\epsilon k_2 z}.$$

Consider an ensemble of atoms at given position and time, and moving with axial velocities in the narrow interval between v and v + dv. In a coordinate system in which the ensemble is at rest the incident fields appear as $E_1'(z, t)$ and $E_2'(z, t; \epsilon)$, with E_j' identical to Eqs. (1) except that due to the Doppler effect,

$$\Omega_1 \rightarrow \Omega_1' = \Omega_1 - k_1 v \quad ,$$

$$\Omega_2 \rightarrow \Omega_2' = \Omega_2 - \epsilon k_2 v \quad ; \tag{2}$$

$$k_j \rightarrow k_j' = \Omega_j' / c \quad .$$

Note that in this section z and t always refer to the coordinates in the moving frame. The total Hamiltonian for the system is

$$H = H_o + V(t) \quad , \tag{3}$$

where H_o is the Hamiltonian of an isolated atom with stationary states $\psi_j(\vec{R})$ of energy $\hbar W_j$:

$$H_o \psi_j = \hbar W_j \psi_j \quad , \quad j = 0, 1, 2 \quad . \tag{4}$$

The ensemble is coupled to the applied fields by the interaction Hamiltonian

$$V(t) = -\mu E'(z, t) \quad , \tag{5}$$

in which μ is the electric dipole operator and $E' = E_1' + E_2'$. The time evolution of a particular member of the ensemble is determined by its wave function Ψ, which may be expanded in terms of the stationary states ψ_j:

$$\Psi(\vec{R}, t) = \sum_{j=0}^{2} e_j(t)\, \psi_j(\vec{R}) \quad , \tag{6}$$

with $e_j(t)$ the probability amplitude of level j. The equations of motion for the e_j's may be obtained in the usual manner by inserting Eqs. (3)-(6) into the time-dependent Schrödinger equation $H\Psi = i\hbar\partial\Psi/\partial t$, multiplying on the left by ψ_i^*, and integrating over all space $(\vec{R})$. Going over to the interaction picutre by means of the transformation

$$c_j(t) = e_j(t) e^{iW_j t} \quad , \tag{7}$$

one obtains:

$$\dot{c}_i = \sum_j a_{ij} c_j \quad ; \tag{8}$$

in which

$$a_{ij} = -\frac{i}{\hbar} V_{ij} e^{i(W_i - W_j)t} \quad ; \tag{9}$$

$$V_{ij} = -\mu_{ij} E'(\vec{r}, t) \quad . \tag{10}$$

(In the above equations $\vec{R}$ indicates the electron coordinates in the atom's reference frame and $\vec{r}$ is the position vector of the atom's center of mass in the moving frame.)

Equation (8) describes the evolution of an undamped atom. The effects of radiative decay may be included[21] by modifying (8):

$$\dot{c}_i = \sum_j (a_{ij} - \frac{1}{2}\gamma_j \delta_{ij}) c_j \quad . \tag{11}$$

Note that in the absence of applied fields (11) leads to exponential decay of level j with decay rate γ_j:

$$|c_j(t-t')|^2 = |c_j(t')|^2 e^{-\gamma_j (t-t')} \quad . \tag{12}$$

Equation (11) may be simplified by the substitution

$$d_j(t) = c_j(t) e^{+\frac{1}{2}\gamma_j t} \quad , \tag{13}$$

which yields a set of coupled equations of exactly the form of the undamped equations of motion (8):

$$\dot{d}_i = \sum_j b_{ij} d_j \quad , \tag{14}$$

with

$$b_{ij} = a_{ij} e^{\frac{1}{2}(\gamma_i - \gamma_j)t} \quad . \tag{15}$$

The system of equations (11) [or its equivalent, (14)] must be solved subject to the appropriate initial conditions. Generally speaking, immediately after its creation the wave function of an atom is a mixture of stationary states with arbitrary phase factors. The random nature of these phase factors, however, makes possible the assumption that the atoms are produced in the pure states, levels 0, 1 and 2. In considering the excitation of these levels one may distinguish between transitions induced by the applied fields and background excitation arising from incoherent processes. The latter are responsible for populating the levels at rates which may be assumed to be independent of the applied fields;[22] accordingly, background atoms are produced in level k at a rate $n_k \gamma_k$, where n_k is the number of atoms with velocity component v in level k in the absence of applied fields.

We adopt the notation $c_j(t;t_o, k)$ to indicate a solution to (11) for an atom produced in level k at t_o.[23] The appropriate boundary conditions are:

$$c_j(t_o;t_o, k) = \delta_{kj} e^{i\psi_j}, \tag{16}$$

in which the φ_j's are unimportant arbitrary phase factors. The transition probability to another level, level j, at subsequent time t is $|c_j(t;t_o, k)|^2$. The probability of an atom in level j decaying in the interval between t and t + dt is $\gamma_j dt$. Thus, for an atom produced in level k at t_o, the transition rate to level j is:[24]

$$\gamma_j |c_j(t;t_o, k)|^2. \tag{17}$$

Considering that the rate of production of atoms in level k is $n_k \gamma_k$, the ensemble-averaged transition rate between levels k and j is:

$$n_k \gamma_k \gamma_j \int_{-\infty}^{t} |c_j(t;t_o, k)|^2 \, dt_o = n_k J_{kj} , \tag{18}$$

which defines J_{kj}, the ensemble-averaged k→j transition rate per atom produced in level k.

In order to estimate the net emitted power induced by E_1', all events in which a photon is emitted or absorbed at Ω_1' must be considered: An atom which is produced in level 2 and subsequently decays from level 1 at rate J_{21} must, by necessity of energy conservation, exchange two photons with the applied fields, a photon absorbed at Ω_2' and a photon emitted at Ω_1' [Fig. 2(a)]. In contrast, an atom which is produced in level 0 and subsequently decays from level 1 at rate J_{01} must emit a

single photon at Ω_1'. An atom produced in level 1 absorbs photons at Ω_1' by the reverse processes, namely, single-quantum transitions from levels 1 to 0 and double-quantum transitions from levels 1 to 2. The net rate of emission of photons at Ω_1' is therefore

$$\mathcal{R} = n_2 J_{21} + n_0 J_{01} - n_1 (J_{10} + J_{12}) \quad , \tag{19a}$$

and the corresponding power emitted is:

$$I_\nu(\Omega_1') = \hbar \Omega_1' \mathcal{R} \quad . \tag{19b}$$

Note that in the limit of $E_2' \to 0$, J_{21} and J_{12} should vanish, and J_{01} and J_{10} should reduce to the usual transition rates for a two level system.

In the formulation presented here the elementary act of transition from level k at t_o to level j at t is described in terms of its corresponding transition probability, $|c_j(t; t_o, k)|^2$. It is evident on very general grounds that the reverse act of transition is equally probable:

$$|c_j(t; t_o, k)|^2 = |c_k(t; t_o, j)|^2 \quad . \tag{20}$$

This point is discussed further in Appendix A. It immediately follows that $J_{kj} = J_{jk}$, and (19a) simplifies to

$$\mathcal{R} = (n_2 - n_1) J_{21} + (n_0 - n_1) J_{01} \quad , \tag{21}$$

a convenient form for calculation.

It is worth noting that Eq. (19) utilizes the fact that the atomic ensemble on the average exchanges electromagnetic energy with E_1 in units of $\hbar \Omega_1'$. This is interesting, since throughout our formulation we have dealt with classical fields exclusively. In fact, in calculating the

emitted power it is not necessary to explicitly introduce the concept of field quanta; instead, one may evaluate[3] the expectation value of the induced dipole moment, $\int \Psi^* e \vec{R} \Psi d^3R$. Then the ensemble-averaged polarization at Ω'_j for atoms produced in level k is

$$P_j^k(t) = n_k \gamma_k \int_{-\infty}^{t} 2 Re \left[\mu_{j0} e_j^*(t; t_o, k) e_0(t; t_o, k) \right] dt_o \quad , \qquad (22)$$

and the net power emitted is

$$I_\nu(\Omega'_j) = - < \sum_k \dot{P}_j^k(t) E'_j(z, t) >_{\text{time average}} \quad . \qquad (23)$$

In Appendix B, using density matrix notation, it is shown that Eq. (23) leads to $I_\nu(\Omega'_1) = \hbar\Omega'_1 \mathcal{R}$, Eq. (19b), where $\mathcal{R}$ is identical to Eq. (19a). This is accomplished by calculating the power emitted or absorbed by atoms produced in particular levels, starting from Eq. (22). For instance, in this way it is shown that for atoms produced in level 2 [Fig. 2(a)], the emitted power at Ω'_1 is given by $\hbar\Omega'_1 n_2 J_{21}$, while for atoms produced in level 0 it is given by $\hbar\Omega'_1 n_0 J_{01}$.

We proceed to calculate the emitted power in terms of transition rates, Eq. (21). The explicit form of the equations of motion (14) are:

$$\dot{d}_0 = \alpha^* e^{i\delta_1 t} d_1 + i\beta e^{i\delta_2 t} d_2 \quad , \qquad (24a)$$

$$\dot{d}_1 = i\alpha e^{-i\delta_1 t} d_0 \quad , \qquad (24b)$$

$$\dot{d}_2 = i\beta^* e^{-i\delta_2 t} d_0 \quad , \qquad (24c)$$

in which

$$\alpha = \mu_{10} A_1/\hbar \quad ,$$
$$\beta = \mu_{02} A_2^*/\hbar \quad , \tag{25}$$

and $i\delta_k = i(\omega_k - \Omega_k') + \frac{1}{2}(\gamma_0 - \gamma_k)$. In writing (24) anti-resonant terms have been neglected, since their influence is negligible when $\langle \mu E \rangle << \hbar\omega_j$. From Eqs. (13) and (16), the appropriate boundary conditions are seen to be

$$d_j(t_o; t_o, k) = \delta_{kj}\, e^{\frac{1}{2}\gamma_j t_o + i\varphi_j} \quad . \tag{26}$$

A solution to this set of equations for all values of E_2 and for weak E_1 may be obtained by means of a simple perturbation technique.[10] This procedure, however, involves lengthy expressions. To present the important steps in a concise manner, a number of symbols are introduced. For the convenience of the reader, these are collected in Table I. Additional details regarding the perturbation technique will be found in Appendix A.

Consider an atom produced in either level 0 or 2: In the absence of coupling through α (i.e. $\alpha = 0$), (24b) yields $d_1 = 0$, while (24a) and (24c) reduce to the equations of motion of a damped, two level system. The solution is straightforward: for an atom initially in level 2,

$$d_0^u(t;t_o,2) = \frac{\beta\, d_2(t_o;t_o,2)\, e^{i\delta_2 t_o}}{s}\left(e^{iq_+T} - e^{iq_-T}\right) , \qquad (27a)$$

$$d_2^u(t;t_o,2) = \frac{d_2(t_o;t_o,2)}{s}\left(q_+ e^{-iq_-T} - q_- e^{-iq_+T}\right) . \qquad (27b)$$

In these equations the superscript u designates the parameters of the uncoupled system and $T = t - t_o$, $s = \sqrt{\delta_2^2 + 4|\beta|^2}$ and $q_\pm = \frac{1}{2}(\delta_2 \pm s)$. By virtue of symmetry, $d_0^u(t;t_o,0)$ may be obtained from $d_2^u(t;t_o,2)$ by replacing $d_2(t_o;t_o,2)$ by $d_0(t_o;t_o,0)$ and $q_\pm$ by $-q_\mp$. For $\alpha \neq 0$, d_1 no longer vanishes: an approximate expression, complete to lowest order in α, may be obtained by integrating (24b) with d_0 replaced by d_0^u:

$$d_1(t;t_o,k) \cong i\alpha \int_{t_o}^{t} e^{-i\delta_1 t'}\, d_0^u(t';t_o,k)\, dt'; \quad k = 0, 2 . \qquad (28)$$

For an atom initially in level 2, substitution of (27a) into (28), and using (13), yields:

$$c_1(t;t_o,2) = \frac{\alpha\beta}{s} e^{-\frac{1}{2}\gamma_1 T} e^{-i\{(\Omega_{21}' - \omega_{21})t_o - \varphi_2\}} \left\{ \frac{e^{i\eta_+ T} - 1}{\eta_+} - \frac{e^{i\eta_- T} - 1}{\eta_-} \right\}, \qquad (29)$$

in which $\Omega_{21}' = \Omega_2' - \Omega_1'$, $\omega_{21} = \omega_2 - \omega_1$, and $\eta_\pm = q_\pm - \delta_1$. Similarly, $c_1(t;t_o,0)$ may be obtained by substituting $d_0^u(t;t_o,0)$ into (28);one finds:

$$c_1(t;t_o,0) = \frac{\alpha}{s} e^{-\frac{1}{2}\gamma_1 T} e^{i\{(\Omega_1' - \omega_1)t_o + \varphi_0\}} \left\{ \frac{q_+\left[e^{i\eta_- T} - 1\right]}{\eta_-} - \frac{q_-\left[e^{i\eta_+ T} - 1\right]}{\eta_+} \right\}, \qquad (30)$$

TABLE I: Symbols Used in Calculation of Transition Rates, Eqs. (31) and (32)

$$\Omega'_{21} = \Omega'_2 - \Omega'_1 \qquad \alpha = \mu_{10} A_1 / \hbar$$

$$\omega_{21} = \omega_2 - \omega_1 \qquad \beta = \mu_{02} A_2^* / \hbar$$

$$d_j(t; t_o, k) = c_j(t; t_o, k)\, e^{\frac{1}{2}\gamma_j t} \qquad T = t - t_o$$

$$i\delta_k = i(\omega_k - \Omega'_k) + \frac{1}{2}(\gamma_0 - \gamma_k) \qquad q_{\pm} = \frac{1}{2}(\delta_2 \pm s)$$

$$s = \sqrt{\delta_2^2 + 4|\beta|^2} \qquad \eta_{\pm} = q_{\pm} - \delta_1$$

In accordance with (18), J_{01} and J_{21} may be obtained by integrating $|c_1|^2$, obtained from Eqs. (29) and (30), over t_o; one finds:

$$J_{21} = \gamma_1 \gamma_2 \frac{|\alpha|^2 |\beta|^2}{|s|^2} \operatorname{Re} \left\{ \frac{1}{|\eta_+|^2} \left[\frac{1}{\gamma_1} + \frac{1}{\gamma_1 - i(\eta_+ - \eta_+^*)} - \frac{2}{\gamma_1 - i\eta_+} \right] \right.$$

$$+ \frac{1}{|\eta_-|^2} \left[\frac{1}{\gamma_1} + \frac{1}{\gamma_1 - i(\eta_- - \eta_-^*)} - \frac{2}{\gamma_1 - i\eta_+} \right] \qquad (31)$$

$$\left. - \frac{2}{\eta_+^* \eta_-} \left[\frac{1}{\gamma_1} + \frac{1}{\gamma_1 - i(\eta_- - \eta_+^*)} - \frac{1}{\gamma_1 - i\eta_-} - \frac{1}{\gamma_1 + i\eta_+^*} \right] \right\} ;$$

$$J_{01} = \gamma_0 \gamma_1 \frac{|\alpha|^2}{|s|^2} \operatorname{Re} \left\{ \frac{|q_-|^2}{|\eta_+|^2} \left[\frac{1}{\gamma_1} + \frac{1}{\gamma_1 - i(\eta_+ - \eta_+^*)} - \frac{2}{\gamma_1 - i\eta_+} \right] \right.$$

$$+ \frac{|q_+|^2}{|\eta_-|^2} \left[\frac{1}{\gamma_1} + \frac{1}{\gamma_1 - i(\eta_- - \eta_-^*)} - \frac{2}{\gamma_1 - i\eta_-} \right] \qquad (32)$$

$$\left. - \frac{2 q_-^* q_+}{\eta_+^* \eta_-} \left[\frac{1}{\gamma_1} + \frac{1}{\gamma_1 - i(\eta_- - \eta_+^*)} - \frac{1}{\gamma_1 - i\eta_-} - \frac{1}{\gamma_1 + i\eta_+^*} \right] \right\}$$

The constituent terms of (31) and of (32) may be combined and simplified in a straightforward (though lengthy) manner to obtain:

$$J_{21} = 2 |\alpha|^2 |\beta|^2 \operatorname{Im} \left\{ \frac{L_2 - 2 \frac{\gamma_{20}}{\gamma_0} R}{AB} \right\} ; \qquad (33)$$

$$J_{01} = -2 |\alpha|^2 \operatorname{Im} \left\{ \frac{R}{B} + |\beta|^2 \frac{L_2 - 2 \frac{\gamma_{20}}{\gamma_0} R}{AB} \right\} . \qquad (34)$$

Here,

$$A = |L_2|^2 + \frac{4\gamma_{20}^2}{\gamma_0\gamma_2}|\beta|^2 \quad , \tag{35a}$$

$$B = -R L_1^* + |\beta|^2 \quad , \tag{35b}$$

$$L_1' = \Delta_1' + i\gamma_{10} \quad , \tag{36a}$$

$$L_2 = -\Delta_2' + i\gamma_{20} \quad , \tag{36b}$$

$$R = (\Delta_1' - \Delta_2') - i\gamma_{21} \quad , \tag{36c}$$

$$\Delta_j' = \Omega_j' - \omega_j \quad , \tag{37}$$

and

$$\gamma_{ij} = \frac{1}{2}(\gamma_i + \gamma_j) \quad . \tag{38}$$

As expected, for $|\beta|^2 \to 0$, J_{21} approaches zero while J_{01} reduces to $2|\alpha|^2 \gamma_{10}/|L_1|^2$, the usual expression for the $0 \to 1$ single-quantum transition rate. Accordingly, the laser field manifests itself through two separate radiative acts: 1), it gives rise to a double-quantum transition rate J_{21}; 2), it modifies the single-quantum transition rate J_{01}. As discussed in Section IIIA, below, for Ω_1' tuned close to ω_1 and Ω_2' close to ω_2 the magnitude of J_{21} is of the same order as J_{01}^{β}, the β-dependent portion of J_{01}. At detuned frequencies, however, J_{21} may be considerably larger than J_{01}^{β}. In fact, at detuned frequencies J_{21} reduces to the familiar expression[25] for Raman transitions between levels 2 and 1. [See Section IIIA for further details.]

Having obtained explicit expressions for J_{21} and J_{01}, the net rate of emission at Ω_1' in the moving frame follows from Eq. (21):

$$\mathcal{R} = 2|\alpha|^2 \, \mathrm{Im}\mathcal{D}(v,\epsilon) \quad , \tag{39}$$

$$\mathcal{D}(v,\epsilon) = (n_1 - n_0)\frac{R}{B} + (n_2 - n_0)|\beta|^2 \, \frac{L_2 - 2\frac{\gamma_{20}}{\gamma_0} R}{AB} \tag{40}$$

As in previous notation, the variable ϵ specifies whether E_1 and E_2 propagate in the same direction ($\epsilon = +1$) or in opposite directions ($\epsilon = -1$). In the laboratory rest frame photons are emitted with energy $\hbar\Omega_1$. Thus, in that frame the contribution to the emitted power from atoms moving with axial velocity v is

$$\hbar\Omega_1 \, 2|\alpha|^2 \, \mathrm{Im}\mathcal{D}(v,\epsilon) \quad . \tag{41}$$

Setting all the γ_j equal, (41) reduces identically to expressions obtained in Ref.10, where hard collisions were introduced as the mechanism of decay. The detailed features of that line shape have been fully verified[26] in the microwave region where velocity broadening is negligible. The reader is referred to Refs. 10 and 26 for additional details.

In the formulation presented above the saturation effects manifest themselves as nonlinear intensity dependences of the transition rates. The level populations, n_j, enter into the expression for the net emission rate through the background excitation rates $n_j\gamma_j$, which are assumed independent of the applied fields.[27] Nevertheless, the ensemble averages of these

populations, $\bar{n}_j$, do depend on the intensities of the applied fields. These average populations may be computed in a straightforward manner by considering the average number of atoms found in level j due to production of atoms in all possible initial levels k:

$$\bar{n}_j = \sum_k n_k \gamma_k \int_{-\infty}^{t} |c_j(t; t_o, k)|^2 \, dt_o = \frac{1}{\gamma_j} \sum_k n_k J_{kj} \quad . \tag{42}$$

The right hand expression immediately follows from the definition of J_{kj}, Eq. (18). It should be noted, however, that the average level populations $\bar{n}_j$ do not enter explicitly into the expressions for the power emitted or absorbed at Ω_1' and Ω_2'. That these quantities are related to the net rate of photon emission may be seen as follows: It is shown in Appendix B [Eq. (B 19b)] that the transition rates are connected by the relation,

$$\gamma_j = \sum_k J_{jk} \quad . \tag{43}$$

This equation is merely a restatement of the steady-state condition: Rate of production into level j equals net rate of decay from all levels. Equations (42) and (43) may be combined to yield

$$\sum_k (n_k J_{kj} - n_j J_{jk}) = (\bar{n}_j - n_j) \gamma_j \quad . \tag{44}$$

For j = 1, the left hand side is just $\mathcal{R}$, Eq. (19a). Accordingly, this expression may be interpreted as the steady-state form of a rate equation for the population of level 1,

$$\dot{\bar{n}}_1 = 0 = (n_1 - \bar{n}_1)\gamma_1 + \mathcal{R} \quad , \tag{45}$$

underscoring the fact that emission and absorption of photons must be accompanied by atomic decay.

As pointed out earlier, an equivalent way of calculating the emitted power at Ω_1' is to solve the ensemble-averaged density matrix equations of motion in the steady state and obtain the induced polarization. In the latter approach one does not generally distinguish between single-quantum and double-quantum processes. Also, the solution of the density matrix equations involves algebraic manipulations quite different from those used above. This approach is presented in Appendix C. The method of solution is more or less standard, except that in the perturbation approach employed one of the applied fields may be taken as arbitrarily large. The final results are, of course, in complete agreement with Eq. (39).

B. Doppler-Broadened Response

Having obtained the power emitted by the atoms moving with axial velocity v, it is now necessary to sum over the entire distribution of axial velocities, thus obtaining $I(\Omega_1;\epsilon)$, the total emitted power at Ω_1:

$$I(\Omega_1;\epsilon) = 2\hbar\Omega_1 |\alpha|^2 \, \mathrm{Im} \int_{-\infty}^{\infty} \mathcal{D}(v,\epsilon)\, dv \quad . \tag{46}$$

In carrying out the velocity averages it is convenient to introduce $G_j(v)$, the velocity distribution of atoms in level j:

$$n_j = N_j G_j(v) \quad , \qquad \int_{-\infty}^{\infty} G_j(v)\, dv = 1 \quad , \tag{47}$$

with N_j the total number of atoms in level j. To an incident light beam of propagation constant k the frequency breadth associated with G_j may be characterized by a "Doppler width" ku_j, with u_j as the most probable speed of G_j. Where the velocity distributions are thermalized, the $G_j(v)$'s are Maxwellian. In some applications of Laser-Induced Doppler Line Narrowing, however, the velocity distributions are non-thermal and may even deviate considerably from Gaussian form. (See, in particular, discussions of the atomic oxygen laser, Refs. 3, 7, and 20.) In general, the integrals involved in obtaining (46) depend upon the specific form of the G_j's. Nevertheless, because in the present case we are considering the fully Doppler-broadened limit $\gamma/ku \ll 1$ [u and γ characterized the magnitudes of the most probable speeds (u_j's) and the natural widths (γ_j's), respectively] the resonant behavior of $I(\Omega_1;\epsilon)$ becomes largely independent of the G_j's and it is possible to perform the averages without recourse to their specific form.

The velocity averages are carried out in detail in Appendix D. Briefly, the velocity dependence of $\mathfrak{D}(v;\epsilon)$, which enters through $L_1(\Omega_1')$ and $L_2(\Omega_2')$, Eq (36a,b), and $R(\Omega_1', \Omega_2')$, Eq. (36c), as well as n_j, Eq. (47), is rather complicated in its present form; therefore, as a first step, $\mathfrak{D}$ is rewritten in a form consisting of terms having velocity dependence of the type

$$H_j^{\pm}(v) = G_j(v) \int \left[(\omega + i\gamma) + kv \right] \left[(\omega' + i\gamma') \pm k'v \right] \Big\}^{-1} , \qquad (48)$$

in which ω, ω', γ and γ' are real and γ and $\gamma' > 0$. As shown in Appendix D, in the Doppler limit $\gamma/ku \ll 1$,

$$\int_{-\infty}^{\infty} H_j^- (v)\, dv = \frac{-(2\pi i/k)\, G_j\left(\frac{\omega}{k}\right)}{(\omega + i\gamma) + \frac{k}{k'}(\omega' + i\gamma')} \tag{49a}$$

and

$$\int_{-\infty}^{\infty} H_j^+ (v)\, dv = 0 \quad . \tag{49b}$$

Using Eqs. (49) and then recombining the velocity averaged terms, one obtains a remarkably simple expression for the total emitted power at Ω_1':

$$I(\Omega_1; \epsilon) = 2\pi\hbar c |a|^2 \left\{ w_{01}(\Delta_1/k_1) - 2\frac{\omega_1}{\omega_2}\frac{|\beta|^2}{\gamma_0 Q} w_{02}(\Delta_2/k_2)\, \mathrm{Im} \frac{1}{\left[\Delta_1 - \epsilon\frac{\omega_1}{\omega_2}\Delta_2\right] - i\left[\gamma_{10} + \frac{\omega_1}{\omega_2}\gamma_{20} Q - \frac{\gamma_0}{2}(1+\epsilon Q)\right]} \right\}. \tag{50}$$

Here, $\omega_j = ck_j$,

$$w_{ij}(v) = N_i G_i(v) - N_j G_j(v) \quad , \tag{51}$$

$$\Delta_j = \Omega_j - \omega_j \quad , \tag{52}$$

Q is the factor by which the saturated levels of the 0 - 2 transition are broadened:

$$Q = \left[1 + \frac{4|\beta|^2}{\gamma_0 \gamma_2}\right]^{1/2} \quad , \tag{53}$$

and ϵ specifies whether E_1 and E_2 propagate in the same direction ($\epsilon = +1$) or in opposite directions ($\epsilon = -1$).

Equation (50) predicts a sharp Lorentzian decrease (for $N_0 > N_2$) superimposed upon the broad gain profile, an effect due to the nonlinear coupling of $E_1(z, t)$ and $E_2(z, t; \epsilon)$. The center frequency and width of this resonant decrease are dependent upon the relative propagation directions of the applied fields. When E_1 and E_2 propagate in the same direction ($\epsilon = +1$ case) the change signal is detuned from ω_1, the center of the 0-1 Doppler profile, by an amount $\Delta_1 = \frac{\omega_1}{\omega_2} \Delta_2$ and is of width

$$\Gamma_N = \gamma_1 + \left[\frac{\omega_1}{\omega_2} (\gamma_0 + \gamma_2) - \gamma_0 \right] Q \quad . \tag{54}$$

On the other hand, when E_1 and E_2 propagate in opposite directions ($\epsilon = -1$ case) the change signal appears at a frequency detuned from ω_1 by $\Delta_1 = -\frac{\omega_1}{\omega_2} \Delta_2$ and is of width

$$\Gamma_B = \gamma_1 + \left[\frac{\omega_1}{\omega_2} (\gamma_0 + \gamma_2) + \gamma_0 \right] Q \quad , \tag{55}$$

which is broader than Γ_N by $2\gamma_0 Q$, twice the saturated width of the middle level. The frequencies at which the $\epsilon = +1$ and $\epsilon = -1$ change signals occur have the following significance. Due to the Doppler effect, each applied field couples resonantly only to atoms within a narrow band of velocities. Referring to Eq. (2), it can be seen that E_1 resonates with atoms of velocity near v_1, given by $\Omega_1 - k_1 v_1 = \omega_1$. Similarly, E_2 resonates with atoms of velocity near v_2, given by $\Omega_2 - \epsilon k_2 v_2 = \omega_2$. In general, the velocity bands centered at v_1 and v_2 are distinct and do not overlap. However, at particular frequencies of the applied fields, the two bands will merge into a single one. Equating v_1 and v_2 for $\epsilon = \pm 1$, this condition is

seen to be

$$\Delta_1 = \epsilon \frac{\omega_1}{\omega_2} \Delta_2 \quad , \tag{56}$$

which is the location of the center frequency of the corresponding change signal.

Evidently, the applied fields can couple to each other most effectively when they resonate with the respective transitions of atoms within a narrow band of velocities. Complete substantiation of this point follows from a detailed inspection of the frequency behavior of the rest frame response--determined by the corresponding transition rates--for a particular atomic velocity band. A full discussion is deferred to Section IIIA. Several remarks, however, may be useful at this time. A glance at Eqs. (33) and (34) reveals that J_{21} and J_{01} are rather complicated functions of Ω_1' and Ω_2'. Furthermore, the frequency characteristics of J_{01} are quite different from those of J_{21}. In the fully Doppler-broadened limit, however, a number of simplifying cancellations occur and many details of the responses of individual velocity bands average out. In fact, in this limit the velocity-averaged $2 \rightarrow 1$ transition rate becomes equal to the negative of the β-dependent portion of the $0 \rightarrow 1$ transition rate, a fact responsible for the particularly simple form of the final expression for the emitted power, Eq. (50).

Despite the fact that the $\epsilon = +1$ and $\epsilon = -1$ change signals are symmetrically located about the 0 - 1 center frequency, the corresponding widths

differ. This asymmetry results from the resonant behavior which enters J_{21} and J_{01} through the quantity $R = [(\Omega_1' - \Omega_2') - \omega_{12}] - i\gamma_{21} = [(\Omega_{12} - \omega_{12}) - i\gamma_{21}] - v(k_1 - \epsilon k_2)$. Note that in contrast to L_1 and L_2, the velocity dependence of R differs strongly for $\epsilon = +1$ and $\epsilon = -1$, particularly if ω_1 and ω_2 are comparable. For example, in the important case in which $|\omega_2 - \omega_1| v/c \ll \gamma_{21}$, $R\{\epsilon = +1\}$ becomes essentially velocity independent, while $R\{\epsilon = -1\}$ remains strongly velocity dependent. Bearing this fact in mind, the different widths of I_N and I_R can be understood by inspecting (33) and (34). See Section IIIA for further details.

As discussed in Appendices C and D, the preceeding remarks also apply to the other level configurations of interest. For example, the expression for emitted power for the "V" configuration [Fig. 2(b)], which is the inverted version of the level scheme treated in this section, is given by the negative of Eq. (50), as one might expect. Equation (50) also describes the power emitted by the cascade configuration [Fig. 2(c)] when the factor ϵQ appearing in the imaginary part of the denominator is changed to $-\epsilon Q$. This has the interesting consequence of interchanging the positions of the broad and narrow change signals (for a given value of Ω_2), a "geometrical" effect arising from the different way in which the fields couple to a cascade system.

C. Extension to Standing-Wave Fields

The extension of the above considerations to cases where one or

both of the applied fields are in the form of standing waves is straightforward. As discussed above, nonlinear coupling occurs when two (or more) travelling-wave fields, at least one of which can saturate its transition, are Doppler-shifted into resonance with the same narrow velocity band of atoms. As noted in the introduction, each standing-wave field may be decomposed into travelling-wave components of equal amplitude propagating in opposite directions. As long as the strong field is detuned from the center of its broad Doppler profile (i.e., $|\Omega_2 - \omega_2| > \gamma_{20}$), its components resonate with atoms in distinct bands symmetrically located about the center of the velocity distribution. (In this respect the tuning of a weak standing-wave field is unimportant, since its travelling-wave components cannot couple to one another.) Then the nonlinear coupling can occur only when the frequencies of the applied fields are such that one of the travelling-wave components of the intense field and one of the weak field are Doppler-shifted into resonance with the same band of atoms. One such possibility couples together travelling waves propagating in the same directions and will be recognized as the $\epsilon = +1$ condition of Eq. (56). In addition, there is the possibility of coupling between oppositely-propagating travelling waves, which is just the $\epsilon = -1$ condition of Eq. (56). Consequently, the broad and narrow resonances appear simultaneously, symmetrically located about the 0 - 1 center frequency.

To illustrate the preceding remarks, consider an intense standing-wave field of amplitude $2E_2^0$ and a weak travelling-wave field of amplitude E_1^0 resonating with the respective transitions of a Doppler-broadened three level system. For the present, assume E_2 to be detuned from ω_2. This

situation is directly applicable to the example presented in the introduction where $E_1(\Omega_1)$ probes the lineshape of an optical transition sharing a common level with an oscillating gas laser transition (Fig. 1). For concreteness, suppose the velocity distributions $G_j(v)$ [Eq. (47)] are all Maxwellian at temperature T: In the absence of the laser field ($E_2 = 0$), $\mathcal{P}(\Omega_1)$, the spectrum of power emitted at the probe frequency, is just:

$$\mathcal{P}(\Omega_1) = \mathcal{P}_0(\Omega_1) = (N_0 - N_1)\frac{2\hbar\Omega_1|\alpha|^2}{k_1 u/\sqrt{\pi}}\, e^{-\left(\frac{\Delta_1}{k_1 u}\right)^2}, \qquad (57)$$

which defines $\mathcal{P}_0(\Omega_1)$, the usual expression for power emitted by the Doppler-broadened 0 - 1 transition induced by weak travelling-wave field E_1; here, $u = (2\kappa T/M)^{1/2}$ is the most probable speed, M is the atomic mass, and κ is Boltzmann's constant. In the presence of the laser field, $\mathcal{P}(\Omega_1)$ is strikingly modified: from the $\epsilon = +1$ and $\epsilon = -1$ cases of Eq. (50) one obtains,

$$\mathcal{P}(\Omega_1) = \mathcal{P}_0(\Omega_1)\left\{1 + \frac{N_0 - N_2}{N_0 - N_1}\frac{2|\beta|^2}{\gamma_0 Q}\frac{\omega_1}{\omega_2}\,\mathrm{Im}\left[\frac{1}{(\Delta_1 + \sigma\frac{\omega_1}{\omega_2}\Delta_2) + i\frac{\Gamma_B}{2}} + \frac{1}{(\Delta_1 - \sigma\frac{\omega_1}{\omega_2}\Delta_2) + i\frac{\Gamma_N}{2}}\right]\right\}, \qquad (58)$$

so that narrow and broad change signals identical to those described above for the travelling-wave case appear simultaneously on opposite sides of ω_1. In a number of important applications $\gamma_1 = \gamma_2 \ll \gamma_0$, causing Γ_N and Γ_B to differ enormously.

Equation (58), which was originally presented in Ref. 7 , has been written in a form valid for both cascade ($\sigma = -1$) and "inverted-V" ($\sigma = +1$) coupling configurations, Figs. 2(c) and 2(a), respectively. The corresponding

expression for the "V" level scheme, Fig. 2(b), is given by the negative of (58) with $\tau = +1$. These statements are based on the extension of Eq. (50) to the other coupling schemes, as outlined in Appendix D. See also the remarks at the close of Section IIB.

In the case of weakly saturating laser field, Γ_N reduces to $2(\gamma_{10} + \frac{\omega_1}{\omega_2}\gamma_{20} - \gamma_0)$ and Γ_B to $2(\gamma_{10} + \frac{\omega_1}{\omega_2}\gamma_{20})$, which agrees with expressions previously obtained by other methods.[5, 6] It is easily seen that in that limit, by symmetry, the case of $\omega_2 > \omega_1$ may be obtained by simply interchanging ω_1 and ω_2 in (58).

The interpretation of (58) as it applies to the spontaneous emission version is presented in Section II'B.

Equation (58) is valid as long as the intense standing-wave field is detuned from its atomic center frequency. When both fields are tuned to the centers of their respective gain profiles all of the travelling-wave components can couple to the same atomic velocity band (namely, the one with negligible component of velocity along the z-axis). Consequently, the above considerations, which are based on the coupling of pairs of travelling waves, becomes inadequate. A standing-wave analysis[2] which specifically includes this possibility has described the third-order interaction of E_1 and E_2 for the special case in which levels 1 and 2 of the "V" configuration [Fig. 2(b)] are assumed closely spaced ($|\omega_2 - \omega_1| v/c \ll \gamma$). [Note that the analysis of the cascade configuration, Fig. 2(c), in which the middle level lies about half-way between the other two levels, follows identically.] The analysis[28], based on a density matrix calculation, shows that as E_2 is

tuned close to the center frequency of the 2 - 0 transition an additional contribution to $\mathcal{P}(\Omega_1)$ arises. The latter contribution, however, may be neglected in virtually all cases of interest because it originates in a polarization with spatial variation other than that of the inducing field. Specifically, $P_1(z,t)$, the velocity-averaged polarization at frequency Ω_1 induced by a pair of standing-wave fields $E_1(z,t) = \mathrm{Re}\left\{E_1^o \cos k_1 z \exp i\Omega_1 t\right\}$ and $E_2(z,t) = \mathrm{Re}\left\{E_2^o \cos k_2 z \exp i\Omega_2 t\right\}$ is of the form[2],

$$P_1(z,t) = \mathrm{Re}\left\{X_a \cos k_1 z + X_b \cos(2k_2 - k_1) z\right\} E_1^o e^{i\Omega_1 t}, \qquad (59)$$

where X_a and X_b are the complex susceptibilities associated with the response at Ω_1. The former term is due to the interaction of pairs of travelling-wave components as discussed above, and may be obtained in our treatment from the sum of the ensemble-averaged polarizations $\chi(v, \epsilon = +1)$ and $\chi(v, \epsilon = -1)$ [Eq. (C14)] integrated over velocities. The latter term, in contrast, is due to the coupling of several travelling-wave components and only becomes large when Ω_1 and Ω_2 are tuned close to their respective atomic center frequencies. We are thinking of a polarization induced in a sample cell placed with a resonator. The net emitted power may be obtained from the time average of $\dot{P}_1(z,t) E_1(z,t)$ integrated over the volume of the sample cell. Consequently, the X_a term leads to a contribution to the emitted power identical to the limiting expression of Eq. (58) for $\omega_1 \approx \omega_2$ and $|\beta|^2 \ll \gamma^2$. This contribution is proportional to the length of the sample cell and is independent of its position within the resonator.

In contrast, the contribution due to the X_b term vanishes when the applied fields are detuned several natural widths from their atomic center frequencies. Furthermore, for Ω_1 and Ω_2 tuned close to their center frequencies the latter contribution is highly sensitive to the exact location and length of the sample within the resonator, and in virtually all cases of interest is either negligible for all iocations with'n the resonator, or may be positioned to become so. Inspection of the treatment of Ref. 2 indicates that these conclusions are also applicable for cases where $\omega_1 \neq \omega_2$.

III. APPLICATIONS AND DISCUSSION

In this Part important features of the preceding analysis are illustrated by means of several discussions and applications.

A. Frequency Characteristics of the Rest-Frame Response

It will be recalled that the Doppler-broadened line shape was obtained by summing the ensemble-averaged response of a particular velocity band over the distribution of atomic velocities. This response was formulated in terms of J_{21} and J_{01} [Eqs. (33) and (34)], the transition rates associated with the emission of photons at Ω_1'. Let us now inspect these quantities in the atoms' rest frame, prior to Doppler averaging. To avoid unnecessary detail, consider the limit of these expressions for weakly-saturating E_2 ($|\beta|^2 \ll \gamma^2$). From Eqs. (35) - (38) one finds:[29]

$$J_{21}(\Omega_1', \Omega_2') = 2|\alpha|^2|\beta|^2 \mathrm{Re}\frac{1}{\gamma_0}\left[\frac{1}{L_2 L_1^*} - \frac{1}{R}\left(\frac{1}{L_1^*} + \frac{1}{L_2^*}\right)\right], \quad (60)$$

$$J_{01}(\Omega_1', \Omega_2') = 2|\alpha|^2 \frac{\gamma_{10}}{|L_1|^2} + J_{01}^{\beta}, \quad (61a)$$

$$J_{01}^{\beta} = 2|\alpha|^2|\beta|^2 \mathrm{Im}\left[\frac{1}{RL_1^{*2}} - \frac{i}{\gamma_0}\left(\frac{1}{L_2 L_1^*} - \frac{1}{R}\left\{\frac{1}{L_1^*} + \frac{1}{L_2^*}\right\}\right)\right]. \quad (61b)$$

As explained earlier, J_{21} is the $2 \rightarrow 1$ transition rate, due to double-quantum exchanges with the applied fields; the first term of J_{01} is the $0 \rightarrow 1$ single-quantum transition rate in the absence of E_2; and the second term, which we have denoted as J_{01}^{β}, describes the nonlinear dependence of the $0 \rightarrow 1$ transition rate to lowest order in E_2.

The frequency behavior of J_{21} and J_{01} is determined by the quantities $L_1 = (\Omega_1' - \omega_1) + i\gamma_{10}$, $L_2 = (-\Omega_2' + \omega_2) + i\gamma_{20}$ and $R = (\Omega_1' - \omega_1) - (\Omega_2' - \omega_2) - i\gamma_{21}$ appearing in the denominators of the various terms of (60) and (61). These quantities exhibit distinct types of tunability: L_1^{-1} and L_2^{-1} may be associated with the usual two level behavior, in which one of the applied fields resonates with a pair of energy levels; R^{-1}, on the other hand, involves the frequency of both fields and becomes large when their separation approaches the 2-1 level spacing. Terms involving L_1^{-1} and L_2^{-1} together are strongly enhanced when

$$\left.\begin{aligned} \Omega_1' &\to \omega_1 , \\ \Omega_2' &\to \omega_2 , \end{aligned}\right\} \tag{62}$$

simultaneously, a condition equivalent to Eq. (56), as discussed in Section IIB. Terms in R^{-1} are also enhanced under those conditions. Note, however, that R^{-1} remains resonant for the less stringent condition

$$\Omega_2' - \Omega_1' \cong \omega_2 - \omega_1 , \tag{63}$$

which does not necessitate resonant coupling of the two level type [Eq. (62)]. Close to resonance [Eq. (62)] J_{21} and J_{01}^{β} exhibit different line-shape characteristics. Nevertheless, in this region they are comparable in magnitude. A few natural linewidths away from resonance, however, J_{21} begins to dominate, becoming larger than J_{01}^{β} by a factor $\sim\gamma/|L_1|$. In fact, in this limit J_{21} reduced to the familiar expression for the Raman transition rate,[30]

$$J_{21} \to 2|\alpha|^2|\beta|^2 \frac{\gamma_{21}}{|R|^2|L_1|^2} , \tag{64}$$

and J_{01}^{β} becomes negligible. Thus, double-quantum transitions predominate when level 0 is detuned from resonance. These features have been well substantiated[26] in the microwave region, as stated above.

In considering a pair of applied fields resonating with a broad atomic velocity distribution, it is possible for atoms within a particular velocity band to satisfy condition (62); consequently, in our case J_{01}^{β} and J_{21} contribute comparably to the velocity-averaged response.

The foregoing discussion is directly applicable to the other energy level configurations of interest. Note that in extending these considerations to the cascade case [Fig. 2(c)], the "Raman" condition [Eq. (63)] should be replaced by: $\Omega_1' + \Omega_2' = \omega_1 + \omega_2$. See Appendix C for further details.

So much for the frequency response of a particular velocity band. The Doppler-broadened response is obtained by summing this quantity over the entire distribution of atomic velocities. As pointed out earlier, in the present case these averages [Eq. (46)] have been carried out in the fully Doppler-broadened limit ($\gamma/ku \ll 1$), resulting in a number of cancellations which greatly simplify the final expressions. Thus, in this limit the velocity average of J_{21} becomes identical with the negative of the velocity average of J_{01}^{β}. This may be easily seen in the special case of weak saturation of

the 0-2 transition, Eqs. (60) and (61), where the first term of J_{01}^{β} averaged over a broad distribution of velocities vanishes; the remainder is equal to $-J_{21}$. It is important to point out that such cancellations do not occur in higher orders of γ/ku. For instance, the complete cancellation of γ_0 in Γ_N which occurs in the case of $(\omega_1/\omega_2) \approx 1$ (see Section IIIC, below) does not occur in the next order of γ/ku.

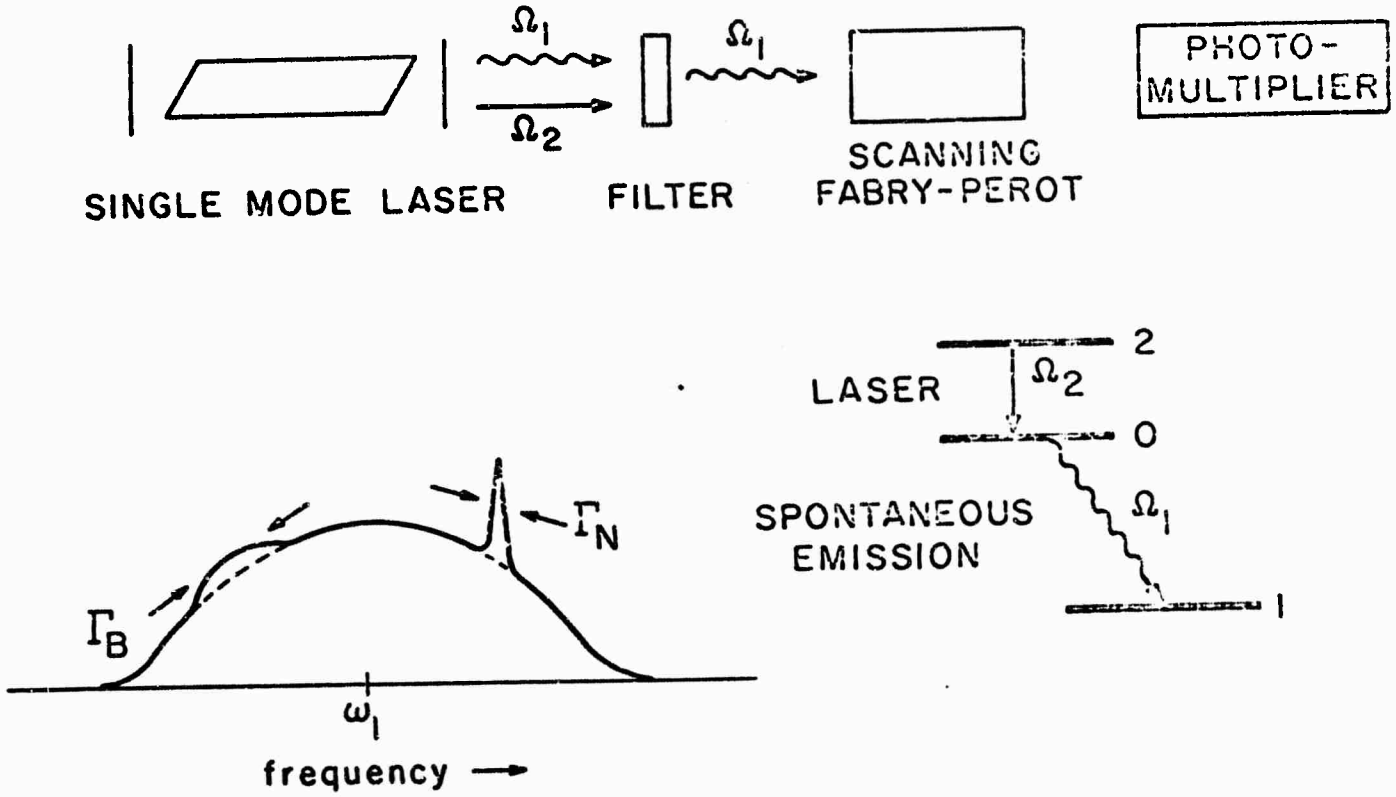

FIGURE 3: Spontaneous Line Narrowing Effect: Simplified Experimental Arrangement, Energy Level Diagram, And Spontaneous Emission Line Shape As Influenced By Laser Field

B. Spontaneous Emission Line Narrowing Effect

We turn next to the manifestation of the Laser-Induced Doppler Line Narrowing Effect appearing in the profile of spontaneous emission from either of the levels of a Doppler-broadened gas laser transition. In this case the interaction of a standing-wave laser field with the 2 - 0 transition (Fig. 3) considerably influences the 0 - 1 profile of spontaneous emission as observed along the laser axis. This influence arises both through single-quantum and double-quantum exchanges with the radiation fields in a manner completely analogous to the induced emission case, and the resulting line shapes are identical. In fact, the 0 - 1 spontaneous emission spectrum follows the spectrum of emission induced by a weak monochromatic probe field tuned through the resonance when the population of level 1 is ignored. Accordingly, Eq. (58) gives the required spontaneous emission spectrum when N_1 is set equal to 0 and $\mathcal{L}(\Omega_1)$ is interpreted as the usual unperturbed Doppler profile ($E_2 = 0$) due to 0 - 1 spontaneous emission. In the quantized field calculation of Ref. 43 the laser-induced spontaneous emission profile is obtained directly. Those results are in exact agreement with the weak saturation limit of our results as they apply to spontaneous emission, given below.

To amplify the foregoing remarks on the applicability of the classical field treatment to the spontaneous emission case, recall the discussions of Section IIA, formulated in terms of the response (in the atoms' rest farme) of a particular velocity band of three level atoms to a weak monochromatic probe field, $E_1'(\Omega_1')$, as influenced by a second field, $E_2'(\Omega_2')$, strongly interacting with the coupled transition. Suppose that the monochromatic probe field is replaced by a wave packet distributed in frequency about Ω_1' over a narrow interval $d\Omega_1' \ll \gamma$ and incident in a given direction within a small solid angle dS: Then all of the considerations of Section II A follow identically, where the field intensity $c E_1^{o\,2}/8\pi$ is interpreted as an average quantity.

Since $d\Omega_1' \ll \gamma$, the response at Ω_1' is independent of the specific form of the frequency distribution of the wave packet. Accordingly, let us express this average field intensity as

$$\frac{c}{8\pi} E_1^{o2} = I\, d\Omega_1'\, dS \quad , \tag{65}$$

where I represents the average intensity per unit frequency interval and solid angle. In terms of $\bar{\nu}$, the average number of light quanta per mode of the (polarized) radiation field, the field intensity becomes

$$I\, d\Omega_1'\, dS = \bar{\nu} \frac{\hbar \Omega_1'^3}{8\pi^3 c^2} d\Omega_1'\, dS \quad . \tag{66}$$

The transition rates, J_{ik}, representing the absorption and induced emission processes described in Section IIA, may therefore be written in terms of $\bar{\nu}$ by replacing E_1^{o2} in Eqs.(33) and (34) by $\bar{\nu}\,(\hbar\Omega_1'^3/\pi^2 c^4)\, d\Omega_1'\, dS$. (Note that E_1^{o2} enters into Eqs.(33) and (34) through $|\alpha|^2$, defined as $|\mu_{10} E_1^o/2\hbar|^2$.) To explicitly emphasize the dependence on $\bar{\nu}$, let us write

$$J_{ik} = \bar{\nu}\, \mathfrak{B}_{ik}\, d\Omega_1'\, dS \tag{67}$$

with $\mathfrak{B}_{ik} = (|\mu_{10}|^2 \Omega_1'^3/4\hbar\pi^2 c^3)\, J_{ik}/|\alpha|^2$. The effect of spontaneous emission at frequency Ω_1' may be included by simply replacing $\bar{\nu}$ by $\bar{\nu} + 1$ in the emission rates, J_{21} and J_{01}.[31] Consequently, for $\bar{\nu} = 0$, the $1 \to 0$ and $1 \to 2$ absorption rates vanish, and the $0 \to 1$ and $2 \to 1$ emission rates reduce to $\mathfrak{B}_{01}\, d\Omega_1'\, dS$ and $\mathfrak{B}_{21}\, d\Omega_1'\, dS$, respectively. Using Eqs.(19a) and (19b) the power spontaneously emitted in frequency interval $d\Omega_1'$ and solid angle dS is seen to be

$$\hbar\Omega_1' \left(n_0 \mathcal{B}_{01} + n_2 \mathcal{B}_{21}\right) d\Omega_1' \, dS \qquad . \tag{68}$$

Note that in this expression the n_1 coefficient has vanished because for $\bar{v} = 0$ the absorption coefficients, $\mathcal{B}_{10}$ and $\mathcal{B}_{12}$, also vanish.

For $|\beta|^2 \to 0$ Eq. (68) reduces to the usual expression for spontaneous emission from the 0 - 1 transition. In applying this formula one should interpret μ_{j0} as $\int \psi_j^*(\vec{R})\, \hat{\epsilon}_j \cdot \vec{\mu}\, \psi_0(\vec{R})\, d^3R$ where $\vec{\mu}$ is the electric dipole operator, $\hat{\epsilon}_2$ is the polarization of the laser field, and $\hat{\epsilon}_1$ is the polarization of a spontaneously emitted photon. Thus, the angular and polarization properties of the spontaneously emitted radiation depend on the characteristics of the particular states involved.

Doppler broadening and standing-wave effects may be included in exactly the same way as in Sections II B and II C, respectively, considering contributions only from that portion of the spontaneous radiation emitted into a small solid angle in the forward (+ z) direction. Thus, as stated above, the spectrum of spontaneous emission from the 0 - 1 transition is given by Eq. (58) with $N_1 = 0$ and $\mathcal{N}(\Omega_1)$ interpreted as the usual Doppler-broadened spectrum of power emitted spontaneously into $d\Omega_1 dS$ with given polarization in the absence of the laser field. Equation (58) has been written in the form valid for both folded ($\sigma = +1$) and cascade ($\sigma = -1$) cases, Figs. 2(a) and 2(c). Suppose, for example, the laser field is tuned to a frequency below its center frequency, ω_2: Then the 0 - 1 spontaneous emission change signals in the cascade case, which result primarily from double-quantum transitions between levels 2 and 1, are in the form of resonant increases, with the I_N resonance above ω_1, the 0 - 1 center frequency, and the I_B resonance below ω_1 (Fig. 3). In the folded case,

on the other hand, the change signals, which primarily result from single-quantum transitions between levels 0 and 1, are in the form of resonant decreases, and the positions of Γ_B and Γ_N are reversed [Fig. 1(b)]. This reversal is a purely geometrical effect arising from the different way in which the fields couple to the respective transitions in the folded and cascade cases. (See Appendices C and D.) Similar conclusions were also obtained in Ref. 4.

Double-quantum transitions are a phenomenon well known since the early days of the quantum theory. Historically, Ehrenfest[32] was the first to suggest a model capable of correctly describing sequential decays among levels. This model was motivated by the correspondance principle and adiabatic theorem of the old quantum theory. Results based on the Ehrenfest model were later found to be in agreement with the quantum-electrodynamical treatment of Weisskopf and Wigner.[33] These ideas were all formulated with spontaneous decay in mind. However, in the presence of an intense field and close to the resonance condition $\Omega_1' = \omega_1$ and $\Omega_2' = \omega_2$, an additional effect becomes important: the intense field can considerably perturb the usual single-quantum emission rate of a coupled transition,[10] an effect comparable in magnitude with the double-quantum emission rate. Older treatments have not been concerned with the former effect; line shape behavior of the kind described in this paper involves an interplay of both types of processes.

It may be illuminating to outline the Ehrenfest picture.[32, 33] Consider the cascade system of Fig. 2(c): following Ehrenfest, assume that when an atom is in level j (energy eigenvalue: $\hbar W_j$), the probability that its energy lies in the interval between $\hbar x$ and $\hbar(x + dx)$ is a Lorentzian centered about $\hbar W_j$ and of width $\hbar\gamma_j$:

$$P_j(x)dx = \frac{\pi(\gamma_j/2)dx}{(W_j - x)^2 + (\gamma_j/2)^2} \tag{69}$$

(normalized to unity). Consider an atom initially in the upper cascade state (level 2) which underwent decay via level 0 to level 1, accompanied by two photons successively emitted at Ω_1' and Ω_2' (in the atom's rest frame): the joint probability that the atom had energies x, y, and z when it was in levels 2, 0, and 1, respectively, is $P_2(x)P_0(y)P_1(z)$. Evidently, the photons emitted in that event were of frequencies $\Omega_2' = x-y$ and $\Omega_1' = y-z$. Substituting Ω_1' and Ω_2' into this probability expression and integrating over all possible values of y, one obtains the total probability of an atom having successively emitted photons at Ω_1' and Ω_2':

$$\int dy \frac{1}{(W_2-\Omega_2'-y)^2 + (\gamma_2/2)^2} \cdot \frac{1}{(W_0-y)^2 + (\gamma_0/2)^2} \cdot \frac{1}{(W_1+\Omega_1'-y)^2 + (\gamma_1/2)^2} . \tag{70}$$

(The unimportant numerical factor has been set equal to unity.) Upon integration (which may be performed as in Appendix D) Eq. (70) yields a result identical in frequency dependence to the lowest order expansion of over $2 \rightarrow 1$ emission rate, Eq. (60) or, equivalently, the expression for $\mathcal{B}_{21}$ obtained from Eq. (67). (Equation (60) is written in general form. See Table II)

A recent discussion[5], formulated on the basis of two-photon transitions induced by a weakly-saturating laser field, has analyzed the frequency profile of spontaneous emission arising from the lower

laser level (Fig. 3). This discussion is presented for the limiting case $\gamma_{21} \rightarrow 0$. It is easily seen that in this limit Eq. (70) involves a δ-function, becoming: $\delta(\Omega_2' + \Omega_1' - \omega_2 \cdot \omega_1)|L_1|^{-2}$; the discussion of Ref. 5 is equivalent to integrating the latter expression over the atomic velocity distribution for $\epsilon = +1$ and $\epsilon = -1$. In addition, Ref. 5 states the line-shape result for arbitrary γ_j, a result in agreement with the weak field limit ($Q \approx 1$) of our expression (58) as it applies to spontaneous emission for $\sigma = -1$ and $N_0 = 0$. The latter result utilizes the Eherenfest model, being obtained by averaging Eq. (70) over velocities.[34]

Such an analysis, however, ignores the important role played by background atoms, N_0, produced in level 0, discussed above. This background population can be sizeable, since in practice the populations of upper and lower laser levels often differs by only a small amount. The extension of Eherenfest's model to include this effect does not follow in an obvious way. To emphasize the significance of the role played by background atoms in level 0, consider a cascade system in which only level 0 is populated (i.e. $N_1 = N_2 = 0$). Then in the rest frame of an atom, an applied laser field at Ω_2' will diminish the transition rate at Ω_1', leading to two holes of width Γ_B and Γ_N superimposed upon the velocity-averaged emission profile--an effect entirely due to the dependence of the single-quantum emission rate on the laser field intensity.

On the other hand, the analysis of Ref. 4 does include the influence of these background atoms, although that treatment does not make explicit the distinction between single-quantum and double-quantum events.

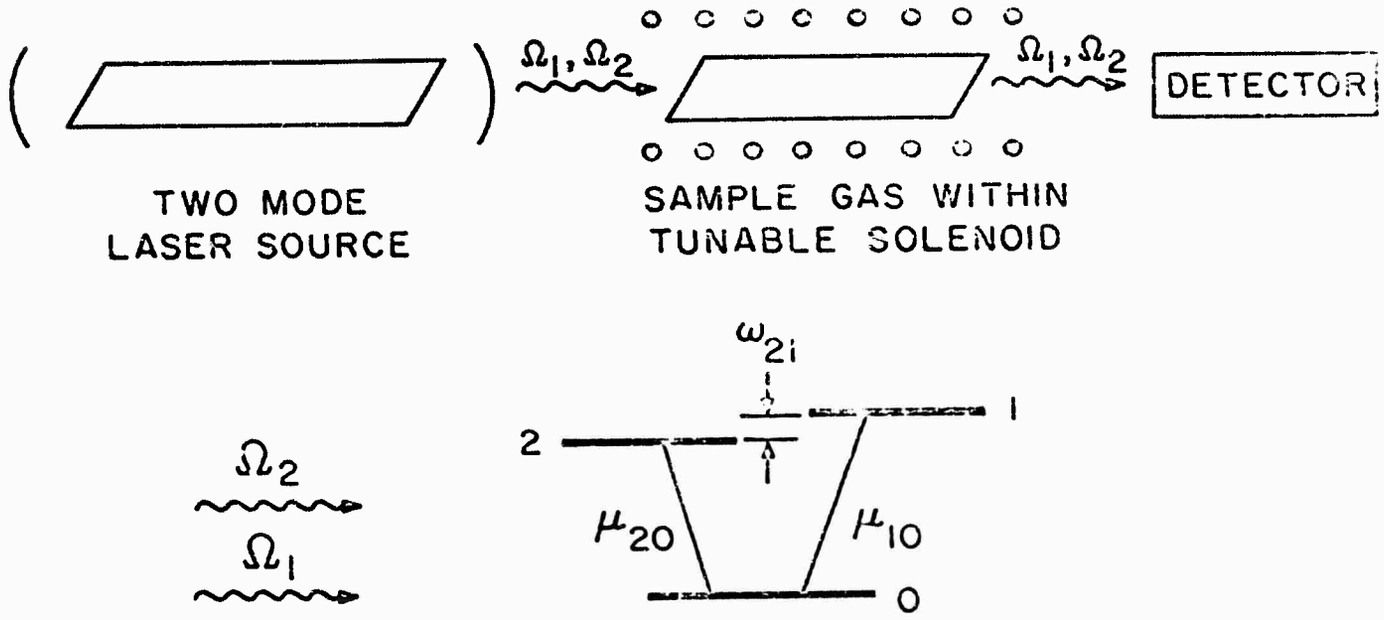

FIGURE 4: Mode Crossing Effect, Simplified Experimental Arrangement And Energy Level Diagram

C. Mode Crossing Experiments

The narrow resonance, Γ_N, is being utilized in a series of precision measurements of hyperfine structure in xenon[12] and G-factors in atomic oxygen[13]. In these experiments ω_1 is close to ω_2 and Γ_N is considerably less than Γ_B. Levels 1 and 2 are a pair of tunable Zeeman components optically coupled to a common level, level 0, and the monochromatic fields E_1 and E_2 are two oscillating laser modes of fixed frequency separation determined by the cavity length. As the Zeeman levels are magnetically tuned, resonant behavior occurs when their splitting approaches the frequency separation between the two laser modes. We shall therefore refer to this effect[11] as "mode crossing". Important aspects of mode crossing have been presented in Ref. 2; some of these are discussed here, for completeness, together with additional details.

A simple version of the mode crossing technique is shown in Fig. 4: The output of a Brewster-angle gas laser oscillating in two modes is attenuated (or amplified) as it passes through a magnetically tunable external sample cell. The respective laser modes should resonate with the two coupled Doppler-broadened transitions of the sample gas. For example, in cases where the laser levels themselves consist of closely spaced tunable components the sample cell may be a discharge tube containing the same gas as the laser tube. The intensity of the transmitted laser beam is studied as a function of the level separation. At low field intensities, where saturation effects are negligible, the attenuation changes slowly as the levels

are tuned, appreciable changes occurring only when the frequency separation of the Zeeman components varies by an amount comparable to the Doppler width. However, when one of the applied fields (ℓ_2) saturates the transition with which it resonates (2 - 0), the attenuation of the coupled transition (1 - 0) undergoes, in addition, a sharp change when the appropriate frequency condition is met. The expression for this behavior is readily obtained from the $\epsilon = +1$ case of Eq.(50) Let us specialize to the limiting case, relevant to mode-crossing studies, in which

$$|\omega_2 - \omega_1| \frac{u}{c} \ll \gamma \quad , \tag{71}$$

where u and γ characterize the magnitudes of the most probable speeds (u_j's) and the natural widths (γ_j's), respectively. Assuming the velocity distributions are all Maxwellian at temperature T, the power emitted or absorbed at Ω_1 in a small length of the sample gas is given by:

$$-\mathcal{A}(\Omega_1)\left[1 - \frac{N_2 - N_0}{N_1 - N_0}\,\frac{2|\beta|^2}{\gamma_0 Q}\,\mathrm{Im}\,\frac{1}{(\Omega_{21} - \omega_{21}) - \frac{i}{2}(\gamma_1 + \gamma_2 Q)}\right] \quad , \tag{72}$$

in which $\mathcal{A}(\Omega_1)$ was introduced in Eq. (57) $\Omega_{21} = \Omega_2 - \Omega_1$, $\omega_{21} = \omega_2 - \omega_1$, and the other symbols were defined in Section II B. The above expression predicts a Lorentzian decrease of width $\Gamma_N = \gamma_1 + \gamma_2 Q$ as the Zeeman splitting, ω_{21}, approaches the mode separation, Ω_{21}. In the limit of weak saturation ($Q \to 1$), (72) reduces to an expression obtained in Ref. 2.

There are two noteworthy features of this behavior: First, that the mode crossing frequency condition depends only upon the separation between the laser modes, being insensitive to their individual frequencies;

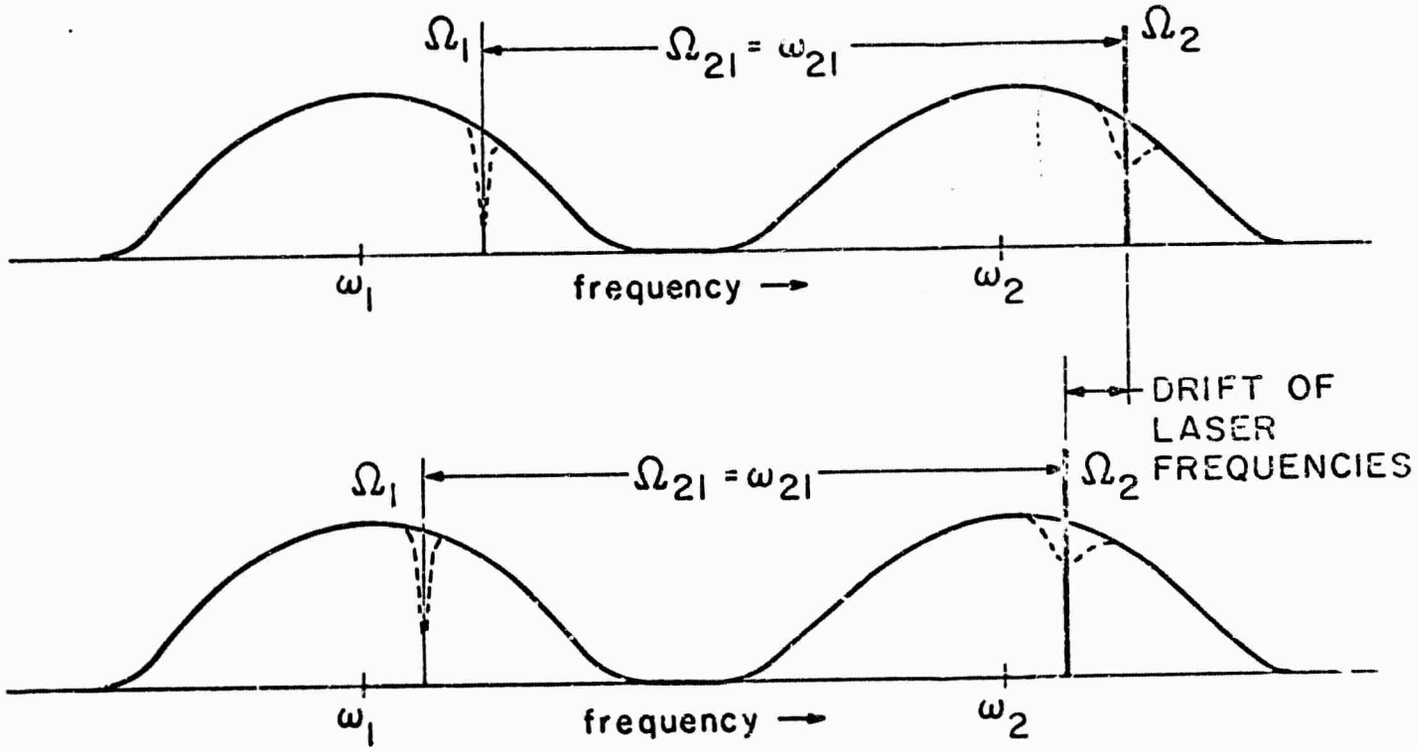

FIGURE 5: Frequency Stability Of Mode Crossing Resonance

and, second, that the width of the mode crossing resonance is the sum of the widths of the "crossing" levels (including power broadening effects), and is essentially independent of the lower level width, γ_0. These two characteristics, which follow from the approximation of closely-spaced crossing levels, (71), have far-reaching implications regarding the required frequency stability and resolution of the mode crossing technique as utilized in precision spectroscopic measurements. In connection with frequency stability, note that although the frequencies Ω_1 and Ω_2 of a free-running laser may wander over a sizeable portion of the broad Doppler profile, $\not\Psi(\Omega_1)$, during the observation time, their separation will remain virtually fixed (see Fig. 5), thereby insuring the stability of the observed signal. In regard to the frequency resolution, note that in many important gas laser applications the widths of the upper levels are much narrower than that of the lower level; the complete cancellation of the latter width in Eq. (72) therefore makes for a relatively narrow signal. This prediction is strikingly born out in mode crossing studies in xenon[12] and oxygen[13], where the observed change signals are not only much narrower than the Doppler width but are also more than an order of magnitude narrower than the known radiative widths of the lower level. It is emphasized that these two simplifying features are characteristic of the approximation of closely-spaced crossing levels,[35] Eq. (71), and do not occur in cases where $\omega_1 \neq \omega_2$.

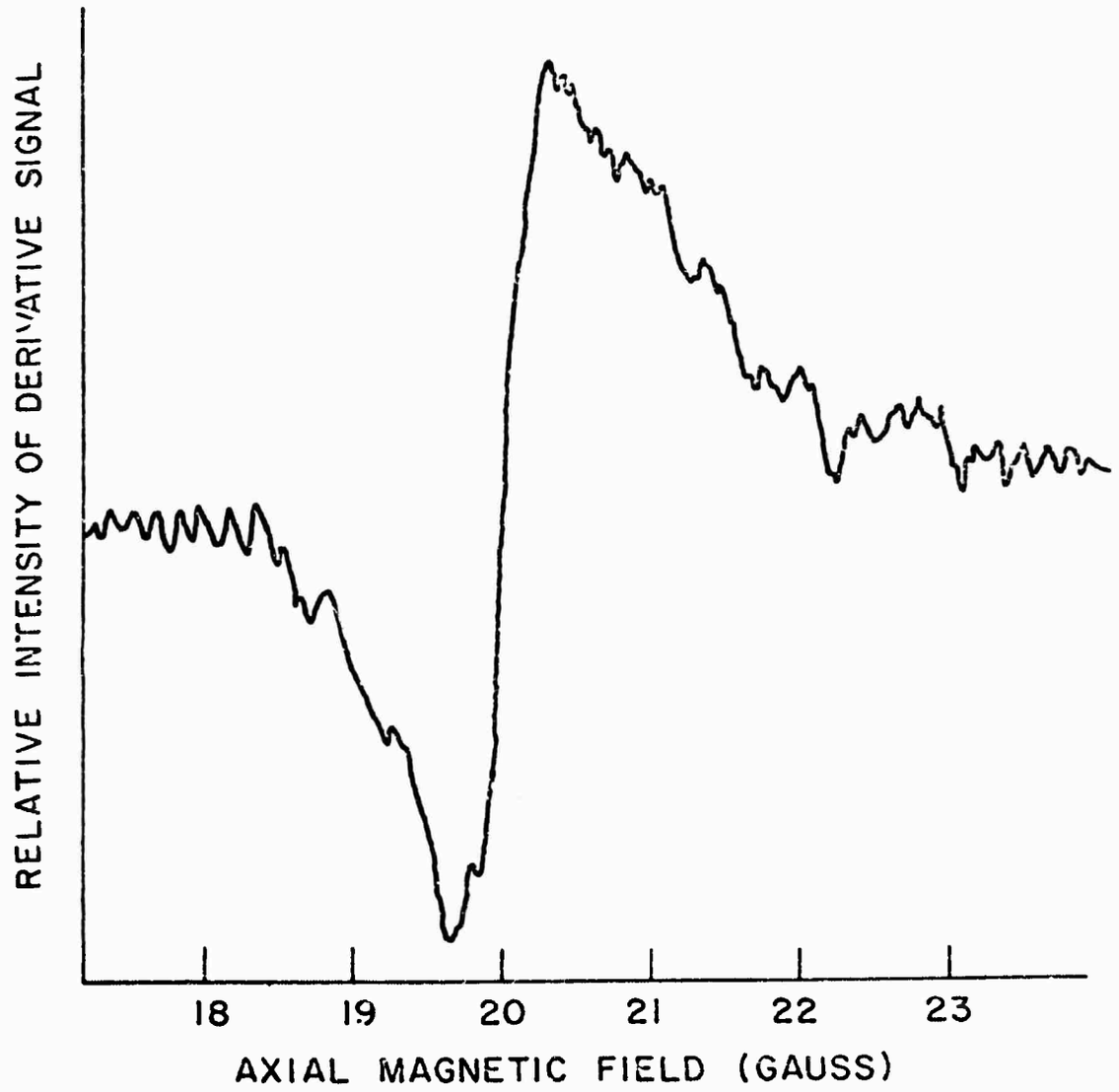

FIGURE 6: Mode Crossing Change Signal Observed In Xe At 3.37 Microns

It should be noted that Eq. (72) holds for the case in which E_1 is weak and E_2 may fully saturate its transition: the case where both fields are intense is not included. Nevertheless, the simple behavior of that expression, as well as Eq. (50), its more general counterpart, is revealing of the effects of high order saturation. It should also be noted that when both fields weakly saturate their respective transitions, the saturated response up to "third-order" may be recovered from (50). This may be achieved by expanding (50) to lowest order in $|\beta|^2$, and noting that there must be symmetry between α and β. Thus, aside from the usual slowly varying third-order background term, the third-order response at Ω_1 is just given by (50) with $Q = 1$, with an analogous expression for the response at Ω_2. This result is in agreement with Ref. 2.

As an example, Fig. 6 depicts a mode-crossing signal observed in xenon at about 20 gauss.[36] The experimental arrangement was similar to the diagram of Fig. 4, except that to enhance the signal-to-noise ratio a small audio frequency component was superimposed on the slowly-varying D.C. axial magnetic field. The detected signal was fed into a phase-sensitive amplifier tuned to the modulation frequency, and the output was recorded as a function of magnetic field. Accordingly, the curve obtained in Fig. 6 is actually the derivative of the mode crossing resonance of Eq. (72). The laser source was a 3.37μ xenon laser[37] with modes separated by about 50 MHz. The crossing levels were pairs of Zeeman components of the upper laser level coupled to a common lower level. The 1 meter magnetically tunable sample cell contained a xenon gas discharge at a pressure of 11μ Hg, so that collision broadening was negligible. The observed g-factor is 0.929; the observed width of 1/2 MHz is consistent

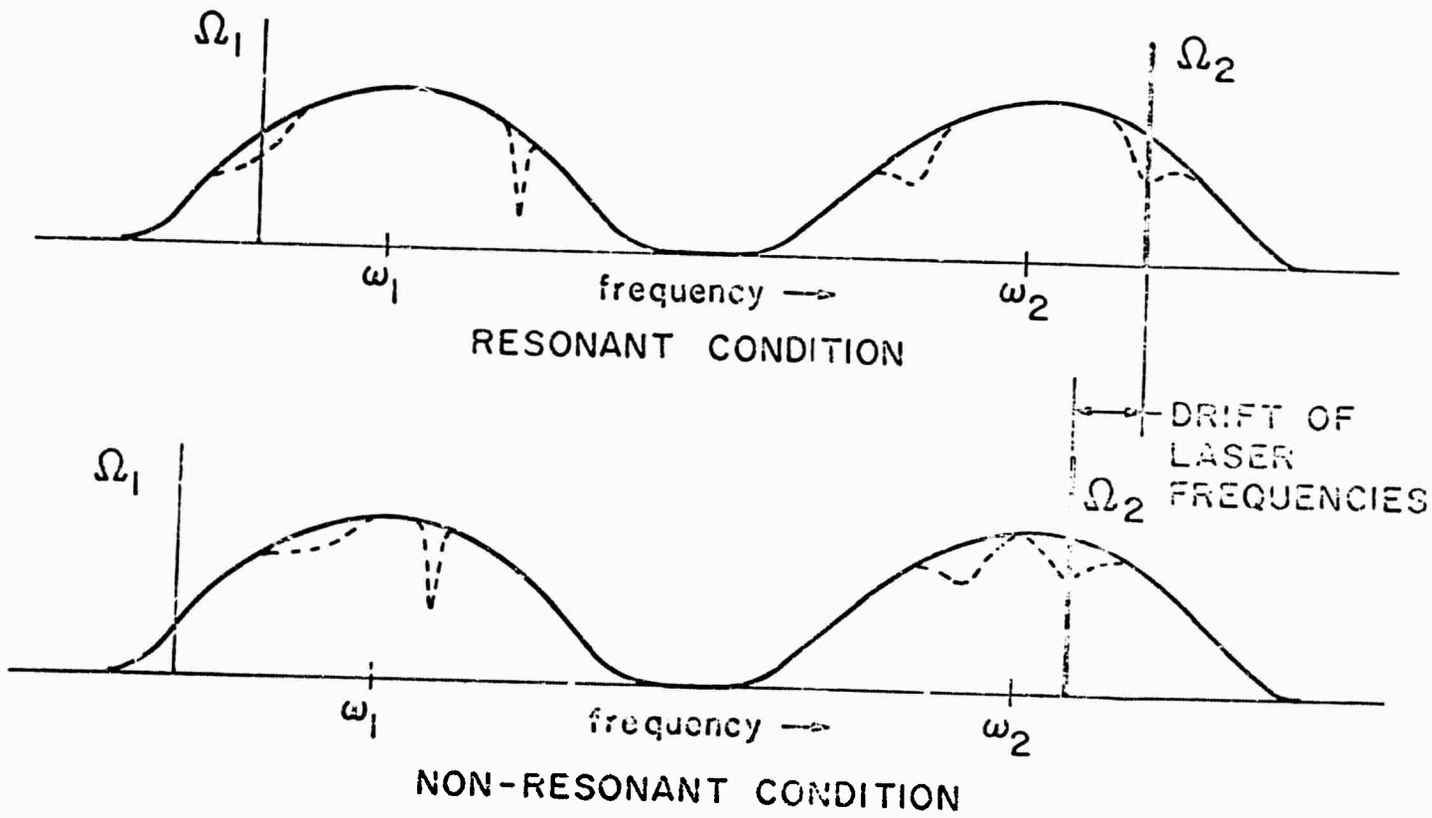

FIGURE 7: Frequency Instability Of The Additional Standing-Wave Resonance Which Occurs When The Sample Cell Is Placed Within The Laser Resonator

with estimates[38] of the upper level of the 3.37μ transition, and about 30 times narrower than that of the lower level.

It is sometimes convenient to place the sample to be studied within the resonator of the laser source, a technique useful, for example, when the laser transition itself consists of closely-spaced tunable levels. As discussed in Section IIC, the standing-wave fields within the laser cavity produce an additional change signal of width Γ_B, due to coupling between oppositely propagating travelling-wave components of E_1 and E_2, symmetrically located about the center frequency from the mode-crossing resonance. (See Fig. 7.) Applying approximation (71) to the expression for Γ_B, Eq. (55), one finds $\Gamma_B = \gamma_1 + \gamma_2 Q + 2\gamma_0 Q$, which can be considerably broader than the mode-crossing resonance (of width Γ_N). The condition for resonance is $\Omega_1 + \Omega_2 = \omega_1 + \omega_2$. In contrast to the frequency condition for mode crossing, this condition is highly sensitive to the absolute frequencies of the individual modes, so that a small instability can cause the modes to drift away from resonance (Fig. 7); consequently, observation of the latter signals would require absolute frequency control as in Lamb-dip experiments.[39]

Finally, we note that in mode-crossing experiments performed within the laser cavity effects due to saturation broadening are enhanced. The overall behavior of these effects is expected to be similar to Eq. (72), i.e., to broaden the resonance by the saturated widths of the crossing levels. Indications of such broadening has been observed in several instances.[13] For example, in mode-crossing experiments performed on the xenon 3.37μ transition within the cavity,[12] the widths observed are generally somewhat broader than that of Fig. 6.

D. Spontaneous Emission Line Narrowing Experiments

The spontaneous emission line narrowing effect has been utilized in measurements of isotope shifts[15] and line width parameters[16] in neon. At the time of the initial observations, a detailed picture of the line narrowing effect predicting differing widths for Γ_N and Γ_B was not at hand. The width difference was not observed in these experiments since in the neon transitions studied, Γ_N and Γ_B differ by only a small amount; its observation requires good laser stability and high finesse Fabry-Perot analysis. The observation of different widths in spontaneous emission in neon has recently been reported by Holt[17].

E. Concluding Remarks

In concluding, we would like to make additional comments concerning several aspects of the Laser-Induced Doppler Line Narrowing Effect.

In the present discussions the atoms have been assumed to relax by means of radiative decay. It should be noted, however, that Eq. (41) and its subsequent average over velocities, Eq. (50), also correctly describe relaxation through hard collisions when the γ_j are interpreted as phase-disrupting hard collision rates. In fact, in the treatment of Ref. 10, which agrees identically with the limiting case of (41) of the γ_j all equal, relaxation was introduced via a single collision rate. The

detailed features of the line shape in that limit have been fully verified[26] in the microwave region, where Doppler effect is negligible and the linewidths are entirely due to collision effects.

On the other hand, in situations where soft collisions--collisions in which phase disruption is incomplete--play an important role, additional details not considered here further influence the line shape. Treatments such as Ref. 40 may be readily extended to this problem. Inclusion of such effects is highly desirable in view of the fact that the pressure dependence of the Laser-Induced Doppler Line Narrowing Effect is observable in a number of rather different experimental contexts. The classical field treatment presented here seems to lend itself more readily to inclusion of collision effects, as opposed to quantized-field treatments.

The line-narrowing effect presented here is also potentially applicable to high-resolution microwave and optical studies of inhomogeneously-broadened solids. In gases the Doppler effect causes the frequency of an applied travelling-wave field to appear different for atoms of different velocities. In solids, on the other hand, the frequency of an incident field appears the same to all of the atoms; instead, inhomogeneity of the crystaline fields may result in a broad distribution of atomic center frequencies. The procedure for including inhomogeneous broadening effects is similiar to the Doppler-averaging procedure employed above. However, since fixed atoms do not discriminate between relative propagation directions of the applied fields, line-narrowing experiments in solids will produce only a single change signal, the analog of the $\epsilon = +1$ change signal observed in a Doppler-broadened gas. Another important distinction is that the simple form

of the relaxation rates introduced into the Schrödinger equation is no longer valid, since non-radiative relaxation mechanisms generally dominate in solids. These may be introduced in a density matrix formalism as in Appendix C by considering appropriate decay constants for the diagonal and off-diagonal density matrix elements. The inclusion of such effects will somewhat modify the characteristics of the observed change signal.

ACKNOWLEDGEMENT

We would like to thank Ted Ducas for checking the manuscript and the calculations.

APPENDIX A: SYMMETRY BETWEEN TRANSITION PROBABILITIES

It is stated in Section II A that $|c_j(t; t_o, k)|^2$, the transition probability of an atom produced in level k at t_o to level j at a later time t, is equal to $|c_k(t; t_o; j)|^2$, the reverse transition probability. This symmetry may be demonstrated by direct calculation. We begin by restating the perturbation technique of Section II A in a more formal manner. The equations of motion for the $d_j(t, t_o, k)$ are given by (24). To obtain a solution for all values of β and $|\alpha| \ll 1$, the d_j may be expanded in powers of α:

$$d_j(t; t_o, k) = d_j^u(t; t_o, k) + \alpha\, d_j'(t; t_o, k) + \alpha^2 d_j''(t; t_o, k) + \ldots \qquad (A\,1)$$

where, as before, the superscript u designates the parameters of the uncoupled system ($\alpha = 0$). We require a solution complete to $O(\alpha)$, consequently only the two leading terms of (A 1) need be retained. Inserting these into (24) and equating coefficients of like powers of α, one obtains the following sets of equations:

$$\dot{d}_0^u = i\beta e^{i\delta_2 t} d_2^u \quad , \qquad (A\,2a)$$

$$\dot{d}_2^u = i\beta^* e^{-i\delta_2 t} d_0^u \quad , \qquad (A\,2b)$$

$$\dot{d}_1^u = 0 \quad ; \qquad (A\,2c)$$

$$\dot{d}_0' = i\frac{\alpha^*}{\bar{\alpha}} e^{i\delta_1 t} d_1^u + i\beta e^{i\delta_2 t} d_2' \quad , \qquad (A\,3a)$$

$$\dot{d}_2' = i\beta^* e^{-i\delta_2 t} d_0' \quad , \qquad (A\,3b)$$

$$\dot{d}_1' = i e^{-i\delta_1 t} d_0^u \quad . \qquad (A\,3c)$$

Equations (A 2a) and (A 2b) are the usual equations of motion a damped, two-level system; (A 2c) is the equation of motion of a third, decoupled level. Equations (A 3) describe coupling effects to lowest order in α.

From (26) and (A 15), the boundary conditions are found to be

$$d_j^u(t_o; t_c, k) = d_j(t_o; t_o, k) \quad ,$$
$$d_j'(t_o; t_o, k) = 0 \quad . \tag{A 4}$$

Thus, for an atom produced in either level 0 or level 2, inspection of (A 2) and (A 3) reveals:

$$d_1^u(t; t_o, k) = 0 \quad , \quad k = 0, 2$$
$$d_j'(t; t_o, k) = 0 \quad , \quad k = 0, 2 \quad , \quad j = 0, 2 \quad : \tag{A 5}$$

Eq. (28) of the text follows immediately from (A 3c).

For an atom produced in level 1, inspection of (A 2) reveals:

$$d_j^u(t; t_o, 1) = d_j(t_o; t_o, 1) \quad . \tag{A 6}$$

Equations (A 3a) and (A 3b) may be combined to yield:

$$\ddot{d}_0' - i\delta_2 \dot{d}_0' + |\beta|^2 d_0' = (\delta_2 - \delta_1)\frac{\alpha^*}{\alpha} d_1(t_o; t_o, 1) e^{i\delta_1 t} \tag{A 7}$$

which may be solved subject to (A 4). Then, noting (A 1) and (A 6), one obtains $d_0(t; t_o, 1)$, complete to $0(\alpha)$:

$$d_0(t; t_o, 1) = \frac{\alpha^* d_1(t_o; t_o, 1)(\delta_2 - \delta_1) e^{i\delta_1 t_o}}{s\left[\delta_1(\delta_2 - \delta_1) + |\beta|^2\right]} \left\{ s\, e^{i\delta_1 T} + \frac{|\beta|^2}{\delta_2 - \delta_1}\left(e^{iq_+ T} - e^{iq_- T}\right) + \left(q_- e^{iq_+ T} - q_+ e^{iq_- T}\right)\right\} . \tag{A 8}$$

The symbols employed above have been defined in Table I. Equation (A 8) may be rearranged to yield:

$$d_0(t; t_o, 1) = \frac{\alpha^*}{s} d_1(t_o; t_o, 1) e^{i\delta_1 t} \left\{ \frac{q_+ [e^{i\eta_- T} - 1]}{\eta_-} - \frac{q_- [e^{i\eta_+ T} - 1]}{\eta_+} \right\} . \quad (A\,9)$$

Inserting (A 9) into (A 3b) and integrating, and noting (A 1) and (A 6), one obtains:

$$d_2(t; t_o, 1) = \frac{\beta^* \alpha^*}{s} d_1(t_o; t_o, 1) e^{i(\delta_1 - \delta_2)t} \left\{ \frac{e^{i\eta_+ T} - 1}{\eta_+} - \frac{e^{i\eta_- T} - 1}{\eta_-} \right\} . \quad (A\,10)$$

Finally, utilizing Eqs. (15), (16), (26), (29) and (30), the symmetry between the probability amplitudes may be displayed:

$$c_0(t; t_o, 1) = \frac{\alpha^*}{\alpha} \frac{c_1(t_o; t_o, 1)}{c_0(t_o; t_o, 0)} \frac{e^{-i(\Omega_1' - \omega_1)t}}{e^{i(\Omega_1' - \omega_1)t_o}} c_1(t; t_o, 0) , \quad (A\,11a)$$

$$c_2(t; t_o, 1) = \frac{\alpha^* \beta^*}{\alpha \beta} \frac{c_1(t_o; t_o, 1)}{c_2(t_o; t_o, 2)} \frac{e^{i(\Omega_{21}' - \omega_{21})t}}{e^{-i(\Omega_{21}' - \omega_{21})t_o}} c_1(t; t_o, 2) . \quad (A\,11b)$$

Notice that from these probability amplitudes on obtains

$$\begin{aligned} |c_0(t; t_o, 1)|^2 &= |c_1(t; t_o, 0)|^2 , \\ |c_2(t; t_o, 1)|^2 &= |c_1(t; t_o, 2)|^2 , \end{aligned} \quad (A\,12)$$

as anticipated in Eq. (20).

APPENDIX B. CONNECTION WITH INDUCED POLARIZATION

In this Appendix the relationship between induced polarization and transition rates is examined.[41] As a convenient starting point, we reformulate the damped equations of motion, Eq. (11), in terms of the density matrix $\rho(t; t_o, k)$, with elements

$$\rho_{ij}(t; t_o, k) = c_i(t; t_o, k)\, c_j^*(t; t_o, k) \quad . \tag{B 1}$$

In keeping with previous notation, $\rho_{ij}(t; t_o, k)$ denotes the value of ρ_{ij} at time t for an atom produced in level k at a prior time t_o, and the c_j's are the probability amplitudes inroduced in Eq. (c). The familiar equation of motion for $\rho(t; t_o, k)$ follows directly from (B1), (7) and (11):

$$\dot{\rho} = -\frac{1}{2}\{\Gamma, \rho\} - \frac{i}{\hbar}[H, \rho] \quad . \tag{B 2}$$

Here [ ] are commutator brackets, { } are anti-commutator brackets,

$$\Gamma_{ij} = \gamma_j \delta_{ij} \quad , \tag{B 3}$$

and H is the total Hamiltonian [Eq. (3)], having matrix elements

$$H_{ij} = \hbar W_j \delta_{ij} + V_{ij} \quad , \tag{B 4}$$

with V_{ij} defined by (10). The expectation value of an operator, such as the induced dipole moment, μ, is

$$p = \mathrm{tr}(\mu \rho) \quad . \tag{B 5}$$

In cases such as the present one, in which the applied fields couple resonantly to different transitions, the equations of motion, (B 2), may be

cast in another form. Inspection of the equations for the off-diagonal elements ρ_{10} and ρ_{20} reveals that in the present case the solutions of interest[42] are of the form

$$\rho_{m0}(t; t_o, k) = \Lambda_m(t - t_o, k)\, e^{i\Omega'_m t}, \qquad m = 1, 2 \quad , \tag{B 6}$$

where the Λ_m are slowly-varying decaying functions of $t - t_o$. Furthermore, inspection of the equations for the diagonal elements shows that the ρ_{jj} are likewise[42] slowly-varying decaying functions of $t - t_o$. [See the discussion of Appendix C, Section 2. These assertions may also be verified directly by forming the $\rho_{ij}(t; t_o, k)$ from Eqs. (27), (29), (30) and (A11).] Then, from (B5), the dipole moment induced at frequency Ω'_m is

$$p_m(t; t_o, k) = \mu_{0m}\rho_{m0}(t; t_o, k) + \text{c. c.} \quad , \tag{B 7}$$

and

$$\dot{p}_m(t; t_o, k) = i\Omega'_m(\mu_{0m}\rho_{m0} - \text{c. c.}) + (\mu_{0m}\dot{\Lambda}_m e^{i\Omega'_m t} + \text{c. c.}). \tag{B 8}$$

Because of the slow variations of the Λ_m, the second term on the right hand side of Eq. (B8) may be conveniently neglected.[43] Using this fact, the diagonal elements of (B2) may be written in the suggestive form:

$$\dot{\rho}_{11}(t - t_o, k) + \gamma_1\rho_{11}(t - t_o, k) = -\frac{1}{\hbar\Omega'_1}\dot{p}_1(t; t_o, k)\, E'(z, t), \tag{B 9a}$$

$$\dot{\rho}_{22}(t - t_o, k) + \gamma_2\rho_{22}(t - t_o, k) = -\frac{1}{\hbar\Omega'_2}\dot{p}_2(t; t_o, k)\, E'(z, t) \quad , \tag{B 9b}$$

$$\begin{aligned}\dot{\rho}_{00}(t - t_o, k) + \gamma_0\rho_{00}(t - t_o, k) = {} & \frac{1}{\hbar\Omega'_1}\dot{p}_1(t; t_o, k)\, E'(z, t) \\ & + \frac{1}{\hbar\Omega'_2}\dot{p}_2(t; t_o, k)\, E'(z, t) \quad .\end{aligned} \tag{B 9c}$$

It is convenient at this point to introduce several definitions and identities. The initial conditions for diagonal and off-diagonal elements of ρ follow from Eqs. (1o) and (7) and may be written:

$$\rho_{ij}(t_o; t_o, k) = \delta_{ik}\delta_{kj} \quad . \tag{B 10}$$

Next, note that

$$\int_{-\infty}^{t} \dot{\rho}_{jj}(t - t_o, k)\, dt_o = -\int_{-\infty}^{t} \frac{\partial}{\partial t_o} \rho_{jj}(t - t_o, k)\, dt_o$$

$$= -\rho_{jj}(t - t_o = 0, k) = -\delta_{kj} \quad , \tag{B 11}$$

by virtue of the boundary conditions. Furthermore, as in Eq. (22) we introduce $P_m^k(t)$, the ensemble-averaged polarization at Ω_m' for atoms produced in level k:

$$P_m^k(t) = n_k \gamma_k \int_{-\infty}^{t} p_m(t; t_o, k)\, dt_o \quad . \tag{B 12}$$

Taking the time derivative of (B12) and noting that (B11) implies $p_m(t_o; t_o, k) = 0$, one obtains:

$$\dot{P}_m^k(t) = n_k \gamma_k \int_{-\infty}^{t} \dot{p}_m(t; t_o, k)\, dt_o \quad . \tag{B 13}$$

Let us inspect Eq. (B9a) as it applies to atoms produced in level 2 ($k = 2$). Multiplying both sides of (B9a) by $n_2\gamma_2 dt_o$ and integrating from $-\infty$ to t using (B11) and (B13), one obtains

$$n_2\gamma_2\gamma_1 \int_{-\infty}^{t} \rho_{11}(t - t_o, 2)\, dt_o = -\dot{P}_1^2(t)\, E'(z, t)/\hbar\Omega_1'$$

$$= -\frac{1}{\hbar\Omega_1'} \langle P_1^2(t)\, E_1'(z, t) \rangle_t + (\text{rapidly varying terms}). \tag{B 14}$$

In this equation the notation $\langle\ \rangle_t$ has been introduced to denote the time average.

On the right hand side of (B14) we retain only the D. C. term -- the remaining terms are not significant and we have systematically ignored contributions of this order.[42] Recalling the expression for the k→j transition rate introduced in Eq. (18),

$$J_{kj} = \gamma_k \gamma_j \int_{-\infty}^{t} \rho_{jj}(t; t_o, k)\, dt_o \quad , \tag{B 15}$$

(B14) yields

$$n_2 J_{21} = -\frac{1}{\hbar\Omega_1'} < \dot{P}_1^2(t)\, E_1'(z, t) >_t \quad . \tag{B 16}$$

The quantity appearing on the left hand side of (B16) was formerly obtained by considering the probability of finding an atom produced in level 2 at t_o in level 1 at a later time t, due to transitions induced by the applied fields. The right hand side of (B16) is the rate at which energy is emitted at frequency Ω_1' in units of $\hbar\Omega_1'$ for atoms produced in level 2. Accordingly, J_{21} represents the rate of photon emission at Ω_1' per atom produced in level 2.

Next, consider Eq. (B9c) for k = 2. A procedure similar to the above results in the expression

$$n_2 J_{20} = \frac{1}{\hbar\Omega_1'} < \dot{P}_1^2(t) E_1'(z, t) >_t + \frac{1}{\hbar\Omega_2'} < \dot{P}_2^2(t) E_2'(z, t) >_t \quad . \tag{B 17}$$

Combining (B14) and (B17), one obtains:

$$n_2 (J_{21} + J_{20}) = \frac{1}{\hbar\Omega_2'} < \dot{P}_2^2(t) E_2'(z, t) >_t \quad . \tag{B 18}$$

The quantity appearing on the left hand side of (B18) was formerly obtained by considering the probability of finding an atome produced in level 2 at t_o in either of the other levels at a subsequent time, due to induced transitions. The right hand side of (B18) is the rate

at which energy is emitted at Ω_2' in units of $\hbar\Omega_2'$ for atoms produced in level 2. Accordingly, $J_{21} + J_{20}$ represents the net rate of photon emission at Ω_2' per atom produced in level 2. Noting that J_{21} is associated with emission of photons at Ω_1' [see Eq. (B16)] and also contributes to photon emission at Ω_2', this emission rate evidently involves exchanges of two quanta with the applied fields. This identification leaves J_{20} as the contribution arising from single quantum exchanges with E_2'.

Equations (B16) and (B18) were derived for atoms produced in level 2. Similar manipulations may be readily extended to the other possible initial conditions. One then obtains the general relations:

$$\hbar\Omega_m' n_k J_{km} = -\langle \dot{P}_m^k(t)\, E_m'(z,t)\rangle_t + \hbar\Omega_m' n_k \gamma_k \delta_{km}, \quad m = 1, 2; \qquad \text{(B19a)}$$

$$\sum_i J_{ki} = \gamma_k \qquad \text{(B19b)}$$

(Note that Eqs. (B19) have been derived under conditions where both fields may fully saturate their respective transitions.) Combining these equations for $m = 1$ and using (23), one finds that the net power emitted at Ω_1' is

$$I_{\nu}(\Omega_1') = \hbar\Omega_1' \left[n_2 J_{21} + n_0 J_{01} - n_1 (J_{12} + J_{10}) \right], \qquad \text{(B20)}$$

which is identical to Eqs. (19) of the text.

APPENDIX C: CALCULATION OF POLARIZATION USING ENSEMBLE-AVERAGED DENSITY MATRIX FORMALISM

This Appendix rederives the results of Section II A of the text by means of the ensemble-averaged density matrix formalism and extends those results to the other coupling configurations. Section C 1 establishes the connection between the time-dependent wave functions and the ensemble-averaged density matrix equations of motion. In Section C 2 these equations are solved for the "inverted-V" configuration, Fig.2(a), and the ensemble-averaged polarization obtained; the same level system was treated in the text by means of the transition rate approach where an equivalent result was, of course, obtained. In Section C 3 the method of Section C 2 is extended to the other level configurations.

1. Equations of Motion

The elements of the ensemble-averaged density matrix corresponding to Eq.(B1) of Appendix B are defined by

$$\rho_{ij}(\vec{r}, t) = \sum_k n_k \gamma_k \int_{-\infty}^{t} \rho_{ij}(t; t_o, k)\, dt_o \quad . \tag{C1}$$

(Note that as we have defined them here, the elements of $\rho(t;t_o, k)$ are dimensionless while the elements of $\rho(\vec{r}, t)$ have the dimension of number of atoms.) Using the relationship

$$\frac{d}{dt}\int_{-\infty}^{t} \rho_{ij}(t; t_o, k)\, dt_o = \rho_{ij}(t\ ; t\ , k) + \int_{-\infty}^{t} \dot{\rho}_{ij}(t; t_o, k)\, dt_o \quad , \tag{C2}$$

and the fact that in the moving frame H, the total Hamiltonian, is independent of t_o, (B2) leads to the familiar differential equation:[44]

$$\dot{\rho}(\vec{r}, t) = \frac{1}{2}\ \{(\rho^o - \rho), \Gamma\} - \frac{i}{\hbar}\ [H, \rho] \quad . \tag{C3}$$

Note that in (C2) the appropriate boundary conditions, from (12), are

$$\rho_{ij}(t_o : t_o, k) = \delta_{ik}\delta_{kj} \quad , \tag{C4}$$

so that in eq. (C3),

$$\rho^o_{ij}(\vec{r}, t) = n_i \delta_{ij} \quad , \tag{C5}$$

with n_j the steady-state background population of level j. Using eq. (C5) and (C1), the ensemble-averaged polarization is

$$\mathrm{tr}\,[\mu\,\rho(\vec{r}, t)] \quad . \tag{C6}$$

2. Ensemble-Averaged Polarization: "Inverted-V" Configuration

We procede to calculate the ensemble-averaged response of a particular velocity band of atoms whose level structure is in the form of an "inverted-V" configuration, as shown in Fig.2(a). From Eq.(C6), the polarization induced by $F'_1(z, t)$ in the moving frame is

$$2\,\mathrm{Re}\,(\mu_{01}\rho_{10}) = \mathrm{Re}\left[\chi(v, \epsilon)\, 2A_1(z) e^{i\Omega'_1 t}\right] \tag{C7}$$

which defines $\chi(v, \epsilon)$, the complex susceptibility for the atoms moving with axial velocity component v.

In the steady state the $\dot{\rho}_{ii} = 0$ except for population fluctuations which are entirely negligible when the $\hbar\Omega'_j >> \langle \mu E' \rangle$. Under these conditions the density matrix equations may be compactly rewritten in the following form:

$$\begin{aligned}
r_{10} &= r^0_{10} + \frac{iE'}{\hbar}\left[\left\{-\frac{\mu_{02}\rho_{20}}{\gamma_0} + \left(\frac{1}{\gamma_1} + \frac{1}{\gamma_0}\right)\mu_{10}\rho_{01}\right\} - \text{c.c.}\right] \\
r_{20} &= r^o_{20} - \frac{iE'}{\hbar}\left[\left\{-\frac{\mu_{10}\rho_{01}}{\gamma_0} + \left(\frac{1}{\gamma_2} + \frac{1}{\gamma_0}\right)\mu_{02}\rho_{20}\right\} - \text{c.c.}\right] \qquad \text{(C8a)} \\
\gamma_0(\rho_{00} - n_0) &+ \gamma_1(\rho_{11} - n_1) + \gamma_2(\rho_{22} - n_2) = 0 \quad ;
\end{aligned}$$

$$\mathcal{L}_{01}\rho_{01} = -\frac{E'}{\hbar}(\mu_{01}r_{10} + \mu_{02}\rho_{21}) \quad ,$$

$$\mathcal{L}_{20}\rho_{20} = +\frac{E'}{\hbar}(\mu_{20}r_{20} + \mu_{10}\rho_{21}) \quad , \qquad \text{(C 8b)}$$

$$\mathcal{L}_{21}\rho_{21} = -\frac{E'}{\hbar}(\mu_{20}\rho_{01} - \mu_{01}\rho_{20}) \quad .$$

In the latter equations $E' = E'_1 + E'_2$ is the net impressed field as seen in the atom's rest frame; we have also introduced the operator

$$\mathcal{L}_{ij} = i\frac{d}{dt} - (W_i - W_j) + i\gamma_{ij} \quad , \qquad \text{(C 9)}$$

and have written $r_{ij} = \rho_{ii} - \rho_{jj}$ and $r^0_{ij} = n_i - n_j$.

This set of equations may be solved by inserting E' in complex form. The various Fourier components of E' drive the off-diagonal elements ρ_{ij}. Of special importance are the coefficients of the ρ_{ij} on the left-hand side of Eqs. (C 8b). These are associated with the resonant behavior of the induced polarization. The only important frequency components of the ρ_{ij} are those which can reduce the magnitudes of their coefficients to the γ_{ij} for particular values of Ω'_1 and Ω'_2. In other words, a nearly exact solution of Eq. 'C 8) can be obtained by assuming the following form for the off-diagonal density matrix components:

$$\rho_{01} = \Lambda e^{-i\Omega'_1 t} \quad ,$$

$$\rho_{20} = \lambda e^{+i\Omega'_2 t} \quad , \qquad \text{(C 10)}$$

$$\rho_{21} = De^{+i(\Omega'_2 - \Omega'_1)t}$$

in which λ, Λ, and D are constants. Inserting (C 10) into Eqs. (C 8), one obtains a set of five simultaneous linear equations:

$$-i(r_{10}-r_{10}^{o}) = \left[-\frac{\beta}{\gamma_0}\lambda + (\frac{1}{\gamma_0}+\frac{1}{\gamma_1})\alpha\Lambda \right] - \text{c. c.} \quad , \tag{C 11a}$$

$$+i(r_{20}-r_{20}^{o}) = \left[-\frac{\alpha}{\gamma_0}\Lambda + (\frac{1}{\gamma_0}+\frac{1}{\gamma_2})\beta\lambda \right] - \text{c. c.} \quad , \tag{C 11b}$$

$$-L_1\Lambda = \alpha^* r_{10} + \beta D \quad , \tag{C 11c}$$

$$L_2\lambda = \beta^* r_{20} + \alpha D \quad , \tag{C 11d}$$

$$R^* D = \alpha^*\lambda - \beta^*\Lambda \quad . \tag{C 11e}$$

The symbols employed here have all been defined in Section II A.

A solution to this set of equations for all values of E_2' and for weak E_1' (i. e. $|\alpha| \ll \gamma$) can be obtained by means of a simple perturbation technique. In the absence of coupling through α the system reduces to a simple two-level system, and the off-diagonal matrix elements ρ_{01} and ρ_{21} vanish. Setting $\alpha = 0$, (C 11) yields the unperturbed solutions:

$$\lambda^u = \frac{r_{20}^{o}\beta^* L_2^*}{A} \quad ,$$

$$r_{10}^{u} = r_{10}^{o} - 2\frac{\gamma_{20}}{\gamma_0}\frac{|\beta|^2 r_{20}^{o}}{A} \quad , \tag{C 12}$$

$$r_{20}^{u} = \frac{r_{20}^{o}|L_2|^2}{A} \quad .$$

In (C 12) the superscript u has been introduced to designate the parameters of the uncoupled system. The presence of coupling through E_1' does not affect the unperturbed parameters λ^u, r_{10}^u and r_{20}^u to lowest order in α. Thus the first order coefficients A' and D' are determined by the first and third off-diagonal equations, (C 11c) and (C 11e):

$$\begin{aligned} -L_1 \; A' &= \alpha^* r_{10}^u + \beta \; D' \quad , \\ R^* \; D' &= \alpha^* \lambda^u - \beta^* \; A' \quad . \end{aligned} \tag{C 13}$$

Equations (C 13), together with (C 12), (C10) and (C 7) yield the complex ensemble-averaged susceptibility complete to first order in α:

$$\chi(\nu, \epsilon) = \frac{\mu_{01} A^*}{A_1(z)} = (n_1 - n_0) \frac{|\mu_{10}|^2 R}{\hbar B} + (n_2 - n_0) \frac{|\mu_{10}|^2}{\hbar} |\beta|^2 \frac{L_2 - 2\frac{\gamma_{20}}{\gamma_0} R}{AB} . \tag{C 14}$$

The time-averaged power emitted at Ω_1' is

$$I_\nu(\Omega_1') = \frac{\Omega_1'}{2} |2A_1|^2 \; \mathrm{Im}\, \chi \; (\nu, \epsilon) \quad ; \tag{C 15}$$

the present result is thus in full agreement with Eq. (39) of Section II A.

3. Extension to Other Level Configurations

The developments of the previous section may be adapted to the other level configurations in a simple and straightforward manner. The configurations of interest are illustrated in Fig. 2. In terms of the relative position of the common level, level 0, they are: the "V" configuration, level 0 lowest [Fig. 2(b)]; the cascade configuration, level 0 between levels 1 and 2 [Fig. 2(c)]; and the "inverted-V" configuration,

level 0 highest [Fig. 2(a)]. The equations of motion, (C8), differ in the various cases only in the relative signs of $W_i - W_j$ which enter into the $\mathcal{L}_{ij}$, Eq. (C 9). These sign changes lead to different choices for the resonant contributions to the off-diagonal density matrix elements, (C 10), which, in turn, necessitate other changes. The modifications of Section C 2 necessary for its extension to the other level configurations are summarized in Table II. Inspection of the final results (noting the definitions of Δ_j' in Table II) reveals that the susceptibility for the cascade and "inverted-V" configurations are the same, except that in the latter case Δ_2' is replaced by $-\Delta_2'$ wherever it appears. Furthermore, the susceptibility for the "V" configuration is the negative of that for the "inverted-V" configuration, a result expected intuitively.

TABLE II. Extension to Other Level Configurations

equation	extended definition
(36a), (36b)	$L_j(y_j) = y_j + i\gamma_{j0}$
(36c)	$R(y_1, y_2) = (y_1 + y_2) - i\gamma_{21}$
(37)	$\Delta'_j = \Omega'_j - \omega_j$
(35a)	$A(y_2) = \lvert L_2(y_2)\rvert^2 + \frac{4\gamma_{20}^2}{\gamma_0 \gamma_2} \lvert\beta\rvert^2$
(35b)	$B(y_1, y_2) = -R(y_1, y_2) L_1^*(y_1) + \lvert\beta\rvert^2$

$$\chi(y_1, y_2) = \frac{\lvert\mu_{10}\rvert^2}{\hbar} \left\{ (n_1 - n_0) \frac{R(y_1, y_2)}{B(y_1, y_2)} + (n_2 - n_0)\lvert\beta\rvert^2 \frac{L_2(y_2) - 2\frac{\gamma_{20}}{\gamma_0} R(y_1, y_2)}{A(y_2) B(y_1, y_2)} \right\}$$

equation	quantity	Level Configuration: "V" [Fig. 2(b)]	"Inverted-V" [Fig. 2(a)]	cascade [Fig. 2(c)]
(C10)	σ_{01}	$A e^{i\Omega'_1 t}$	$A e^{-i\Omega'_1 t}$	$A e^{-i\Omega'_1 t}$
	σ_{20}	$\lambda e^{-i\Omega'_2 t}$	$\lambda e^{i\Omega'_2 t}$	$\lambda e^{-i\Omega'_2 t}$
	ρ_{21}	$D e^{-i(\Omega'_2 - \Omega'_1) t}$	$D e^{i(\Omega'_2 - \Omega'_1) t}$	$D e^{-i(\Omega'_1 + \Omega'_2) t}$
	y_1	$-\Delta'_1$	$+\Delta'_1$	$+\Delta'_1$
	y_2	$+\Delta'_2$	$-\Delta'_2$	$+\Delta'_2$
(25)	α	$\mu_{10} A_1^* / \hbar$	$\mu_{10} A_1 / \hbar$	$\mu_{10} A_1 / \hbar$
	β	$\mu_{02} A_2 / \hbar$	$\mu_{02} A_2^* / \hbar$	$\mu_{02} A_2 / \hbar$
(C14)	$\chi(v, \epsilon)$	$\mu_{10} A / A_1$	$\mu_{01} A^* / A_1$	$\mu_{01} A^* / A_1$
(C14)	$\chi(y_1, y_2)$	$\chi(-\Delta'_1, \Delta'_2)$ $= -\chi^*(\Delta'_1, -\Delta'_2)$	$\chi(\Delta'_1, -\Delta'_2)$	$\chi(\Delta'_1, \Delta'_2)$

APPENDIX D: VELOCITY INTEGRATION IN THE DOPPLER LIMIT

This Appendix presents in detail the velocity integration procedure outlined in Section IIB. As seen in the text, Eq.(41), the expression for the Doppler-shifted response of a particular velocity band of atoms viewed in the laboratory frame, is a rather complicated function of velocity. Moreover, the convolution of such an expression with an atomic velocity distribution $G_j(v)$, Eq. (47), depends, in general, on the specific form of the latter distribution. In the fully Doppler-broadened limit $\gamma/ku \ll 1$, however, it is possible to perform the averages without recourse to the details of the G_j's. Furthermore, a number of cancellations occur in this limit, resulting in a rather simple final expression for the velocity-averaged response.

1. Velocity Integration

As shown in Section 3 of Appendix C, the expressions for the ensemble-averaged response for the various level configurations of interest are closely related to one another. It is worthwhile to perform the velocity averages in a general form, applicable to all of these. Referring to Table II, the susceptibilities for the "V" and "inverted-V" level configurations, Figs. 2(b) and 2(a), respectively, differ only in an overall sign; accordingly, the corresponding velocity averages may be performed identically. Furthermore, the latter expression may be readily extended to the cascade configuration, Fig. 2(c): following Eq. (46), the expression for the Doppler-broadened power spectrum may be written:

$$I_\sigma(\Omega_1;\epsilon) = 2\pi|\Omega_1|\alpha|^2 \operatorname{Im}\int_{-\infty}^{\infty} \mathfrak{D}_\sigma(v;\epsilon)\,dv; \qquad (D1)$$

the subscript σ has been added to denote the "inverted-V" level configuration ($\sigma = +1$), treated in the text, and the cascade configuration ($\sigma = -1$). As in Eq. (40),

$$\mathfrak{D}_\sigma(v;\epsilon) = (n_1 - n_0)\frac{R(\sigma)}{B} + (n_2 - n_0)|\beta|^2 \frac{L_2(\sigma) - 2\frac{\gamma_{20}}{\gamma_0}R(\sigma)}{AB}, \qquad (D2)$$

with

$$A = |L_2(\sigma)|^2 + \frac{4\gamma_{20}^2}{\gamma_0\gamma_2}|\beta|^2 \qquad (D3)$$

and

$$B = -R(\sigma)L_1^* + |\beta|^2 . \qquad (D4)$$

From Table II, the appropriate generalization of Eqs. (36) is

$$L_1 = \Delta_1' + i\gamma_{10} , \qquad (D5a)$$

$$L_2(\sigma) = -\sigma\Delta_2' + i\gamma_{20} , \qquad (D5b)$$

$$R(\sigma) = (\Delta_1' - \sigma\Delta_2') - i\gamma_{21} . \qquad (D5c)$$

To perform the averages, $\mathfrak{D}_\sigma(v, \epsilon)$ is decomposed into its partial fractions. In addition to $n_j = N_j G_j(v)$ [see Eq. (47)], $\mathfrak{D}_\sigma$ is velocity dependent through L_1, L_2, and R, Eqs. (D5). Explicitly,

$\sigma = +1$: "inverted-V" (see text)

$\sigma = -1$: cascade

$\epsilon = +1$: $E_1 \parallel E_2$

$\epsilon = -1$: E_1 anti-$\parallel E_2$

$$l_1 = l_1 - k_1 v \quad , \tag{D6a}$$

$$l_2 = l_2 + \sigma \epsilon k_2 v \, , \tag{D6b}$$

$$R = \Omega - Kv \quad ; \tag{D6c}$$

$$K = k_1 - \sigma \epsilon k_2 \quad ; \tag{D7}$$

$$l_1 = \Delta_1 + i\gamma_{10} \quad , \tag{D8a}$$

$$l_2 = -\sigma\Delta_2 + i\gamma_{20} \quad , \tag{D8b}$$

$$\Omega = (\Delta_1 - \sigma\Delta_2) - i\gamma_{21} \, . \tag{D8c}$$

with $\Delta_j = \Omega_j - \omega_j$. To expedite the decomposition, note that

$$\frac{1}{B} = \frac{1}{g}\left[\frac{1}{k_1 v + b_-} - \frac{1}{k_1 v - b_+} \right] \quad , \tag{D9}$$

in which

$$g = \left[\left(\frac{K}{k_1} l_1^* - \Omega \right)^2 + 4 \frac{K}{k_1} |\beta|^2 \right]^{1/2} \quad , \tag{D10}$$

and

$$b_{\pm} = \frac{1}{2} \frac{k_1}{K} \left| g \pm \left(\frac{K}{k_1} l_1^* + \Omega \right) \right| \quad . \tag{D11}$$

Also,

$$\frac{1}{A} = \frac{i}{2\gamma_{20} Q} \left[\frac{1}{m_- + \sigma \epsilon k_2 v} - \frac{1}{m_+ + \sigma \epsilon k_2 v} \right] , \tag{D12}$$

where

$$m_{\pm} = l_2 - i\gamma_{20}(1 \pm Q) \quad , \tag{D13}$$

and Q is the factor by which the saturated levels of the 0-2 transition are broadened:

$$Q = \left[1 + \frac{4|\beta|^2}{\gamma_0 \gamma_2} \right]^{1/2} . \qquad \text{(D14)}$$

Inserting Eqs. (D9) and (D12) into (D2), the partial fraction decomposition leads to expressions of the form of Eq. (48) of the text:

$$H_j^{\pm}(v) = G_j(v) \left\{ \left[(\omega + i\gamma) + kv \right] \left[(\omega' + i\gamma') \pm k' v \right] \right\}^{-1} , \qquad \text{(D15)}$$

in which ω, ω', γ and γ' are real and γ and $\gamma' > 0$. As stated in Eqs. (49) of the text, in the limit $\gamma/ku \ll 1$,

$$\int_{-\infty}^{\infty} H_j^{-}(v)dv = \frac{-(2\pi i/k') \, G_j(-\frac{\omega}{k})}{(\omega + i\gamma) + \frac{k}{k'}(\omega' + i\gamma')} , \qquad \text{(D16a)}$$

and

$$\int_{-\infty}^{\infty} H_j^{+}(v)dv = 0 . \qquad \text{(D16b)}$$

A proof of Eqs. (D16) will be found at the close of this Appendix. Thus, in the velocity-broadened limit the question of whether or not a particular partial-fraction term of the type (D15) contributes to (D1) is entirely determined by the signs of the imaginary portions of its corresponding factors. Many of these are, in turn, controlled by the sign of K [Eq. (D7)]. We shall confine our attention to the important case in which $K \geq 0$, always valid if either $k_1 \geq k_2$ or $\sigma\epsilon = -1$. The complementary case in which $K < 0$ can be obtained similarly.

It follows from their definitions that when $K > 0$, $\mathrm{Im}(\bar{+}b_{\pm}) > 0$. Using these facts, the velocity-averaged partial fraction components of I_c may be combined to yield:

$$I_\sigma(\Omega_1; \epsilon) = 2\pi\hbar c |\alpha|^2 \left[w_{01}(\Delta_1/k_1) + 2 \frac{k_1}{k_2} \frac{|\beta|^2}{\gamma_0 Q} w_{02}(\Delta_2/k_2) \, \mathrm{Im}F(\sigma\epsilon) \right] , \qquad \text{(D17)}$$

in which

$$F(\sigma\epsilon) = \frac{1}{g}\left[\Omega + \sigma\epsilon\frac{K}{k_2}m_{\sigma\epsilon} - i\frac{\gamma_0}{2}(1+\sigma\epsilon Q)\right]\left[\frac{1}{-\sigma\epsilon\frac{k_1}{k_2}m_{\sigma\epsilon}+b_-} - \frac{1}{-\sigma\epsilon\frac{k_i}{k_2}m_{\sigma\epsilon}-b_+}\right] \quad \text{(D18)},$$

$$w_{ij}(v) = N_i G_i(v) - N_j G_j(v) \quad , \quad \text{(D19)}$$

and

$$\Delta_j = \Omega_j - \omega_j \quad . \quad \text{(D20)}$$

Also, in evaluating the G_j's in (D17) the approximation that $|\beta|^2/\gamma_{21} \ll ku$ has been made.

The first term of (D17) will be recognized as the power emitted by an unsaturated Doppler-broadened two level system. The second term may be simplified by utilizing the identity (D9) with $-\sigma\epsilon(k_1/k_2)m_{\sigma\epsilon}$ substituted for $k_1 v$. Then using (D4) and (D6), (D18) reduces to:

$$F(\sigma\epsilon) = \frac{-\left[\Omega + \sigma\epsilon\frac{K}{k_2}m_{\sigma\epsilon} - i\frac{\gamma_0}{2}(1+\sigma\epsilon Q)\right]}{\left(\Omega + \sigma\epsilon\frac{K}{k_2}m_{\sigma\epsilon}\right)\left(\Omega_1^* + \sigma\epsilon\frac{k_1}{k_2}m_{\sigma\epsilon}\right) - |\beta|^2} \quad , \quad \text{(D21)}$$

which may be further simplified by noting that, inserting (D14) the numerator is a factor of the denomenator. Replacing k_1/k_2 by ω_1/ω_2, slight rearrangement yields.

$$I_\sigma(\Omega_1;\epsilon) = 2\pi\hbar c|\alpha|^2\left\{w_{01}(\Delta_1/k_1) - 2\frac{\omega_1}{\omega_2}\frac{|\beta|^2}{\gamma_0 Q}w_{02}(\Delta_2/k_2)\mathrm{Im}\frac{1}{\left[\Delta_1 - \epsilon\frac{\omega_1}{\omega_2}\Delta_2\right] - i\left[\gamma_{10} + \frac{\omega_1}{\omega_2}\gamma_{20}Q - \frac{\gamma_0}{2}(1+\sigma\epsilon Q)\right]}\right\}, \quad \text{(D22)}$$

a remarkably simple result! For $\sigma = +1$ this expression, of course,

reduces to Eq. (50) of Section IIB.

D2. Proof of Equations (D16)

Consider the integral

$$Z_j(\omega, ku, \gamma) = \int_{-\infty}^{\infty} \frac{k\, G_j(v)dv}{(\omega + i\gamma) + kv}, \qquad (D23)$$

in which ω and γ are real, $\gamma > 0$, and $G_j(v)$ is a slowly-varying, even function of v, of width characterized by u. In the limit $\gamma/ku \ll 1$,

$$(\omega + i\gamma + kv)^{-1} \rightarrow P(\omega + kv)^{-1} - i\frac{\pi}{k}\,\delta\left(\frac{\omega}{k} + v\right), \qquad (D24)$$

where P denotes principle value, and (D23) becomes

$$Z_j(\omega, ku) = P\int_{-\infty}^{\infty} \frac{k\, G_j(v)dv}{\frac{\omega}{k} + v} - i\pi\; G_j\left(-\frac{\omega}{k}\right); \quad \gamma/ku \ll 1. \qquad (D25)$$

For compactness, we shall write

$$Z_j(\omega, ku) = Z_j'(\omega, ku) - i\, Z_j''(\omega, ku) \qquad (D26)$$

with Z_j' and Z_j'' the real and imaginary parts of (D25), respectively.

Consider now the function $H_j^{\pm}(v)$, Eq. (D16): Decomposing $H_j^{\pm}(v)$ into partial fractions and then using (D23), (D25), and (D26), one finds that in the Doppler limit,

$$\int_{-\infty}^{\infty} H_j^{\pm}(v)dv = \frac{\frac{1}{k'}\left[Z_j(\omega' k'u) \mp Z_j(\omega, ku)\right]}{\left(\omega \mp \frac{k}{k'}\omega'\right) + i\left(\gamma \mp \frac{k}{k'}\gamma'\right)}, \quad \gamma/k\,u \ll 1. \qquad (D27)$$

The only significant contribution to (D27) arises from the immediate vicinity of $\omega \mp (k/k')\omega' = 0$. Under the stated assumptions the Z_j vary slowly over this small region; consequently, it is permissible to evaluate the numerator[45] at $\omega = \pm (k/k')\omega'$. Making use of the fact that Z_j' and Z_j'' are odd and even functions of ω, respectively, this substitution leads directly to Eqs. (D16).

REFERENCES

1. W. E. Lamb, Jr., Phys. Rev. 134, A1429 (1964).
2. H. R. Schlossberg and A. Javan, Phys. Rev. 150, 267 (1966).
3. M. S. Feld, Ph. D. Thesis, M. I. T., 1967 (unpublished).
4. G. E. Notkin, S. G. Rautian and A. A. Feoktistov, J. E. T. P. 52, 1673 (1967). [English translation: Soviet Phys. J. E. T. P. 25, 1112 (1967).]
5. H. K. Holt, Phys. Rev. Letters 19, 1275 (1967).
6. M. S. Feld and A. Javan, Bull. Am. Phys. Soc. 12, 1053 (1967).
7. M. S. Feld and A. Javan, Phys. Rev. Letters 20, 578 (1968).
8. R. Bose and J. A. White, Bull. Am. Phys. Soc. 13, 172 (1968).
9. The authors were not aware of the work of Rautian and his collaborators (Ref. 4) at the time Ref. 7 was prepared, and only learned of its existance when the present manuscript was submitted for publication. Accordingly, the manuscript has been revised to acknowledge this substantial work and clarify its connection with our paper and several previous publications.
10. A. Javan, Phys. Rev. 107, 1579 (1957).
11. M. S. Feld, J. H. Parks, H. R. Schlossberg and A. Javan, "Spectroscopy with Gas Lasers", in Physics of Quantum Electronics edited by P. L. Kelley, B. Lax, and P. E. Tannenwald, New York: McGraw-Hill, p. 567 (1966).
12. H. R. Schlossberg and A. Javan, Phys. Rev. Letters 17, 1242 (1966).
13. G. W. Flynn, M. S. Feld and B. J. Feldman, Bull Am. Phys. Soc. 12, 669 (1967).
14. A. Javan, in Quantum Optics and Electronics; Lectures Delivered at Les Houches During the 1964 Session of the Summer School of Theoretical Physics, University of Grenoble, edited by C. DeWitt, A. Blandin, and

Ref. 14 (cont'd) on the next page

Ref. (cont'd)

C. Cohen-Tannoudji (Gordon and Breach Publishers, Inc., New York, 1965), p. 383; J. A. White, J. Opt. Soc. Am. 55, 1436 (1965); see also Ref 1, Section 15.

15. R. H. Cordover, P. A. Bonczyk, and A. Javan, Phys. Rev. Letters 18, 730, 1104(E) (1967).

16. W.G. Schweitzer, Jr., M.M. Birky, and J.A. White, JOSA 57, 1226 (1967).

17. H.K. Holt, Phys. Rev. Letters 20, 410 (1968).

18. W.R. Bennett, Jr., W.L. Faust, R.A. McFarlane and C.K.N. Patel, Phys. Rev. Letters 8, 470 (1962).

19. M.S. Feld, B.J. Feldman and A. Javan, Bull. Am. Phys. Soc. 12, 669 (1967).

20. M S. Feld, B.J. Feldman and A. Javan, "Frequency Shifts of the Fine Structure Oscillations of the 8446-Å Atomic Oxygen Laser," Phys. Rev., to be published.

21. W.E. Lamb, Jr. and R C. Retherford, Phys. Rev. 79, 549 (1950).

22. See Ref. 10 for further details.

23. It might be thought that c_j is also a function of z_0, the position of the moving atom at its time of creation. Note, however, that in the ensemble's rest frame the atoms are stationary: consequently, the position of each member of the ensemble remains fixed (at $z=z_0$) over the entire period of interaction with the applied fields.

24. Note that expression (17) is the rate at which an atom produced in level k makes a coherent transition to level j due to induced emission or absorption, where it decays.

Ref. (cont'd)

25. A. Javan, "Stimulated Raman Effect", in Quantum Electronics and Coherent Light (Proceedings of the International School of Physics "Enrico Fermi," Varenna, Italy) edited by C. H Townes and P. A. Miles, New York: Academic Press, p. 284 (1964).

26. T. Yajima and K. Shimoda, J. Phys. Soc. Japan 15, 1668 (1960); A. P. Cox, G. W. Flynn, and E. B. Wilson, Jr., J. Chem. Phys. 42, 3094 (1965). The latter article contains a number of other relevant references.

27. The latter assumption is not essential and has only been made to simplify the formulation of the problem. Although widely applicable, there are cases where this assumption is not valid. Our approach may be readily modified to include such effects.

28. The expression for the standing-wave polarization given in Ref. 2, Eq. (33), contains a number of errors. The corrected expression is:

$$P_1 = -i\pi^{1/2}/(2ku)$$

$$\times \{(|\mu_{12}|^4/\gamma_1\gamma_2)(N_2-N_1)E_1^3[1+\gamma_{12}[\gamma_{12}-i(\omega_{21}-\nu_1)]^{-1}] \qquad (33a)$$

$$+ (|\mu_{12}|^4/\gamma_1)E_1E_2^2[(\gamma_{12}/\gamma_2)(N_2-N_1)[\gamma_{12}-i(\omega_{21}-\nu_B)]^{-1} \qquad (33b)$$

$$+ (\gamma_{13}/\gamma_3)(N_3-N_1)[\gamma_{13}-i(\omega_{31}-\nu_B)]^{-1}]$$

$$+ (|\mu_{12}\mu_{31}|^2/2\gamma_1)(N_3+N_2-2N_1)E_1^3[\gamma-i(\omega_B-\nu_1)]^{-1} \qquad (33c)$$

$$+ (|\mu_{12}\mu_{31}|^2/2\gamma_1)(N_3-N_1)E_1E_2^2[\gamma-i(\omega_B-\nu_B)]^{-1} \qquad (33d)$$

Ref. 28 (cont'd) on the next page

Ref. (cont' d)

$$+(|\mu_{12}\mu_{31}|^2/\gamma_1)(N_3-N_1)E_1E_2^2[2\gamma - i(\omega_{32}-\Delta)]^{-1}$$
$$[1+\gamma_1[\gamma_{32}- i(\omega_{32}-\Delta)]^{-1}|\}\quad , \tag{33e}$$

$$P_1' = -[i\pi^{1/2}/(4ku)]|\mu_{12}\mu_{31}|^2(N_2-N_1)E_1E_2^2[\gamma_{12}- i(\omega_{21}-\nu_1)|^{-1}$$
$$[\gamma_{32}- i(\omega_{32}-\Delta)]^{-1}\quad . \tag{33f}$$

It should be noted that this expression only holds when the two Doppler gain profiles closely overlap and the laser frequencies are fairly close to their respective center frequencies. More generally, each Lorentzian term is multiplied by a slowly-varying Gaussian. For example, term (33c) vanishes when there is no overlap. A complete Erratum for Ref. 2 is being published concurrently in Phys. Rev.

29. In obtaining these results, the first term of Eq. (34) must be expanded to first order in $|\beta|^2$. In the remainder of (34), which is identical to (33), B^{-1} may be replaced by $(RL_1^*)^{-1}$, and A^{-1} by $|L_2|^{-2} = (i/2\gamma_{20})[(1/L_2)+(1/L_2^*)]$, and specific use is made of the fact that $L_1^* + L_2^* = R - i\gamma_0$.

30. Note that when E_1 and E_2 are detuned from their respective center frequencies by sizable fractions -- a situation which does not concern us here -- additional nonresonant terms which were dropped from the Schrödinger equation (24) may no longer by ignored. For example, we have ignored terms with frequency dependence of the type $(\Omega_1' - \omega_2)^{-1}$.

Ref. 30 (cont' d) on next page

Ref. (cont'd)

Upon inclusion of such terms, one finds that Eq. (64) should be multiplied by the factor $(\omega_2 + \omega_1)(\Omega_2' + \Omega_1')/(\omega_2 + \Omega_1')^2$, which is very close to unity in our case. For a complete discussion of the Raman effect see Ref. 23.

31. It can easily be shown that this procedure leads to results consistent with the requirements of thermal equilibrium, both for 0↔1 single-quantum events and for 2↔1 double-quantum events.

32. P. Eherenfest, Naturwiss 11, 543 (1923).

33. V. F. Weisskopf and E. F. Wigner, Z. Physik 63, 54 (1930).

34. H. K. Holt, Private communication.

35. They also characterize a cascade system in which the middle level lies about half way between the other two levels. (See Appendix D.)

36. We are indebted to Jeff Levine for supplying this trace.

37. W. L. Faust, R. A. McFarlane, C. K. N. Patel and C. G. B. Garrett, Appl. Phys. Letters 1, 85 (1962).

38. F. Horrigan, unpublished.

39. See, for example, A. Szoke and A. Javan, Phys. Rev. 145, 137 (1966), and Ref. 1.

40. B. L. Gyorffy, M. Borenstein and W. E. Lamb, Jr., Phys. Rev. 169, 340 (1968).

Ref. (cont'd)

41. For a related discussion, see L. R. Wilcox and W. E. Lamb, Jr., Phys. Rev. 119, 1915 (1960), Appendix I.

42. These solutions are complete except for rapidly varying perturbations which are negligible for $|\alpha|$ and $|\beta| \ll \omega_1$ and ω_2.

43. This approximation is actually unnecessary and is only made to simplify the algebra. Had the $\dot{A}_m(t - t_o)$ term been retained, it would have dropped out upon averaging over t_o, by virtue of the initial conditions.

44. W. E. Lamb, Jr., and T. M. Sanders, Jr., Phys. Rev. 119, 1901 (1960).

45. When the denominator of (D27) becomes small one should expand $Z_j(\omega', k'u, \gamma')$ about the point (ω, ku, γ). Equation (D16) follows directly.

FIGURE CAPTIONS

Fig. 1. Spectrum of line narrowing induced in the Doppler gain (or attenuation) profiles of (a) laser and (b) coupled transitions. In the energy level configuration depicted the effect takes the form of depletions in gain of the coupled transition over two narrow frequency intervals. As an example, for a weakly saturating laser field and for closely spaced lower levels of equal lifetimes, the broad change signal (width: Γ_B) of the coupled transition is twice as wide as the laser change signals (width:Γ_L), while the narrow change signal (width: Γ_N) is reduced by twice the width of the upper level (level 0) and is independent of it. In the cascade configuration (not shown), level 2 above level 0, change signals of similar widths selectively enhance the background profile of the coupled transition. Also, in the latter case the positions of the two change signals are interchanged.

Fig. 2. Energy level configurations. Frequencies Ω_1 and Ω_2 refer to the applied fields and ω_1 and ω_2 to the level separations. In each case level 0 is common to both 1 - 0 and 2 - 0 transitions.

Fig. 3. Spontaneous line narrowing effect: simplified experimental arrangement, energy level diagram, and spontaneous emission line shape as influenced by laser field. In the latter diagram the laser is assumed to be oscillating somewhat below its atomic center frequency ($\omega - \Omega_2 > \gamma_{20} + \frac{1}{2}\gamma_1$). See text for details.

Fig. 4. Mode crossing effect, simplified experimental arrangement and energy level diagram.

Fig. 5. Frequency stability of mode crossing resonance. The frequency separation of the applied fields, Ω_{21}, remains stable against frequency drift caused by length changes of the laser resonator. Thus the resonant condition $\Omega_{21} = \omega_{21}$ is maintained, regardless of drift of the laser frequencies. Note that in an actual experiment the Doppler prifiles may overlap.

Fig. 6. Mode crossing change signal observed in Xe at 3.37μ. The sample cell is external to the laser resonator (Fig. 4).

Fig. 7. Frequency instability of the additional standing-wave resonance which occurs when the sample cell is placed within the laser resonator. The condition for the latter resonance, $\Omega_1 + \Omega_2 = \omega_1 + \omega_2$, is destroyed by slight fluctuations in resonator length. (Compare Fig. 5.)

A Photoelectric Potential from Photoreceptor Cells in Ventral Eye of Limulus

J. E. Brown, J. R. Murray, and T. G. Smith

ABSTRACT

Intense colored light from a CW gas laser evokes a photoelectric potential (PEP) in the photoreceptor cells of the ventral eye of Limulus. This PEP has two components, both of which have the action spectrum of a 530 nm rhodopsin. The evidence is consistent with the hypothesis that the PEP arises directly from the orderly array of rhodopsin molecules which are an integral part of the photoreceptor cell membrane.

In a previous paper we reported that when the lateral eye Limulus polyphemus is stimulated with very intense lights, a short-latency response can be recorded with intracellular electrodes from the eye's photoreceptor cells (the retinular cells) (1). This electrical response, which we called a photoelectric potential (or PEP), was found to have a number of characteristis similar to the so-called early receptor potential (ERP) studied in vertebrate eyes with extracellular electrodes (2-15). In addition, the observations that the polarity of the PEP reversed across the photoreceptor cell membrane and the amplitude and the polarity of the PEP could be altered by changing membrane potential indicated that the generator of the PEP was intimately associated with the photoreceptor cell membrane (1). However, there remained the questions of whether the Limulus PEP, like the ERP, had two components, and if the spectral sensitivity of these components resembled the absorption spectrum of Limulus rhodopsin. In this paper we present evidence which answers these questions affirmatively.

The present experiments were done on the ventral eye of Limulus. The photoreceptor cells of the ventral eye have many anatomical properties, membrane characteristics and responses to light which are essentially the same as those found in the retinular cell of the lateral eye (17,19). The methods used in these experiments were the same as employed previously (1), with two additions. Here, the action spectra of the PEP were determined by using a CW gas laser (argon or krypton) constructed and

developed by one of us (J.R.M., 16). With this laser, five lines of sufficiently intense monochromatic light within the spectral region of interest were available. The action spectrum of the generator potential was determined by using CW Xenon arc source, narrow-band interference filters and neutral density filters.

When a pulse of white light of moderate intensity (in the range of microwatts) is focused onto a ventral eye photoreceptor cell, the membrane potential undergoes a transient depolarization with the characteristic waveform of the generator potential (Fig.1,A, V_1) and with a latency of several milliseconds (Fig.1A, cf.V_2 and L). When, however, the light intensity is increased several hundred-fold, another response appears whose onset is coincident with the light pulse (Fig.1B, cf.V_2 and L). This response is the PEP.

From Fig. 1,B,V_2, it can be seen that the PEP has two components. The first is a depolarizing potential change which is coincident with the light pulse. The second component is a hyperpolarizing potential change which outlasts the light pulse.

Monochromatic light from the laser produced the same PEP's as those evoked by white light. The action spectra of both components of the PEP fit reasonably well with the absorption spectrum of a rhodopsin (predicted by Dartnall's nomogram) with the absorption maximum taken at 530 nm (20; Fig. 2). Previous studies have shown by microspectrophotometry (18) and with electrophysiological techniques (19) that the absorption spectrum and generator potential action spectrum, respectively, peak near 530 nm. We confirm that the ventral eye generator potential action spectrum peaks near 530 nm (Fig. 2).

In conclusion, we have found that a PEP can be recorded with intracellular electrodes in the photoreceptor cells of the Limulus ventral eye. This PEP is similar, in two more respects, to the ERP recorded extracellularly from vertebrate eyes, viz., there are two components to the response and both components have action spectra which are the same as both the absorption spectrum of rhodopsin and the action spectrum of the generator potential.

We and others (2-15) interpret the presently available evidence to indicate that the PEP and ERP represent an early and perhaps direct electronic change in rhodopsin molecules. Recent evidence suggests that the generation of the ERP is dependent on preservation of an ordered array of rhodopsin molecules (15). Moreover, as will be reported later (17), the properties of the ventral eye PEP, like those of the lateral eye PEP (1), indicate that the PEP generator is an integral constituent of the photoreceptor membrane. Hence, the generators of the ERP and PEP may well be an ordered array of rhodopsin molecules lying in the cell membranes of photoreceptors.

Whether the PEP and ERP are in the direct chain of events leading to the permeability changes associated with the generator potential and ERG, respectively, and if so, how they are coupled to these permeability changes, remain open questions.

REFERENCES

1. Smith, T.G. and Brown, J.E. Nature, 212:1217 (1966).

2. Arden, G.B. and Ikeda, H., Nature, 208:1100 (1965).

3 Brindley, G.S., and Gardner-Medwin, A.R., J.Physiol.,182:185 (1966).

4. Brown, K.T., Nature, 207:1249 (1965).

5. Brown, K.T., and Murakami, M., Nature, 201:626 (1964).

6. Brown, K.T., and Murakami, M., Nature, 204:739 (1964).

7. Brown, K.T., et al., Cold Spr.Harb.Symp. Quant.Biol., 30:457, (1965).

8. Brown, K.T., and Gage, P.W., Fed.Proc., 25;329 (1966).

9. Cone, R.A., Nature, 204:736 (1964).

10. Cone, R.A., Cold Spr. Harb.Symp.Quant.Biol., 30:483 (1965).

11. Pak, W.L., Cold.Spr.Harb.Symp.Quant.Biol., 30:493 (1965).

12. Pak, W.L., and Cone, R. A., Nature, 204:336 (1964)

13. Pak, W.L. and Ebrey, T.G., Nature, 205:484 (1965)

14. Cone, R.A., Science, 155:1128 (1967).

15. Cone, R.A. Science, 156:536 (1967).

16. Murray, John, Unpublished S.B. thesis, MIT Physics Dept. 1965.

17. Smith, T.G. and Brown, J.E. (In preparation).

18. Murray, J.L., Science, 154:1182 (1966).

19. Millecchia, R., et. al., Science, 154:1199 (1966)

20. Dartnall, H.J.A., Brit.Med.Bull., 9:24 (1953).

FIGURE LEGENDS

Fig. 1.

Intracellular responses of Limulus ventral eye to light. In both A and B, V_1 is low gain, D. C. -coupled, slow sweep-speed recording; V_2 is high gain, A. C. -coupled, fast sweep-speed recording; and L is light monitor synchronized with V_2 at the same sweep-speed. In V_2, the initial pulse is a voltage-time calibration marker of 1 mV and 2 msec. The gain of the V_1 trace is 20 times less; the sweep speed 5 times slower. In A, the light intensity was in the range of μ watts. In B, the light intensity was in the range of m watts.

Fig. 2.

Action spectra of the PEP and generator potential. The relative sensitivity (ordinate) against wavelength in nanometers (nm; abscissa). Solid line taken from Dartnall nomogram for 530 nm-pigment. Open circles show the action spectrum of generator potential. Squares and triangles indicate the action spectra of the depolarizing and hyperpolarizing components, respectively, of the PEP.

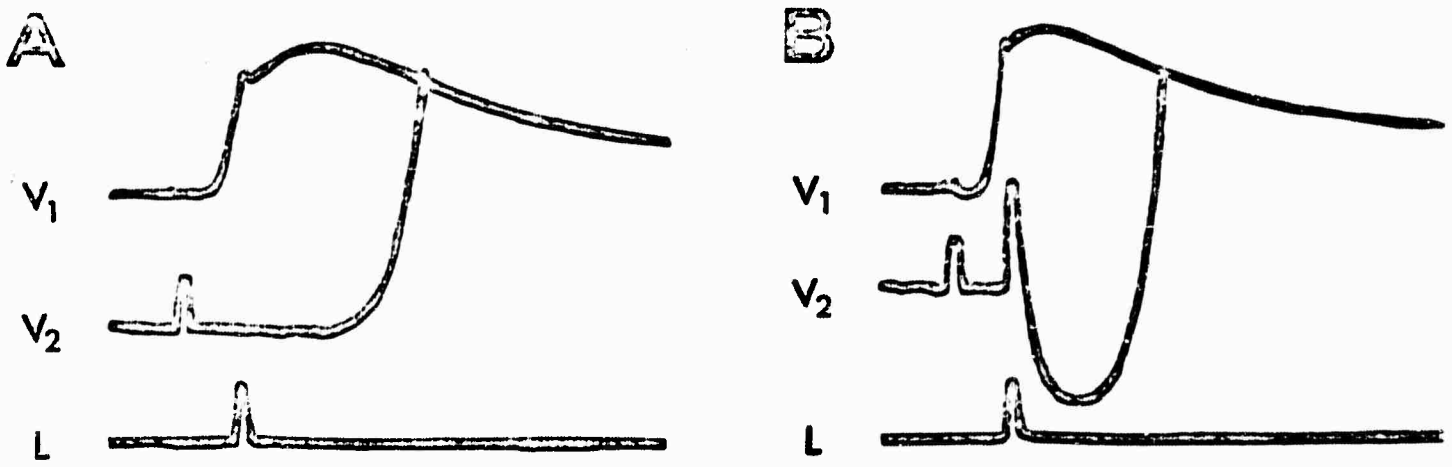
A
V1
V2
L
B
V1
V2
L

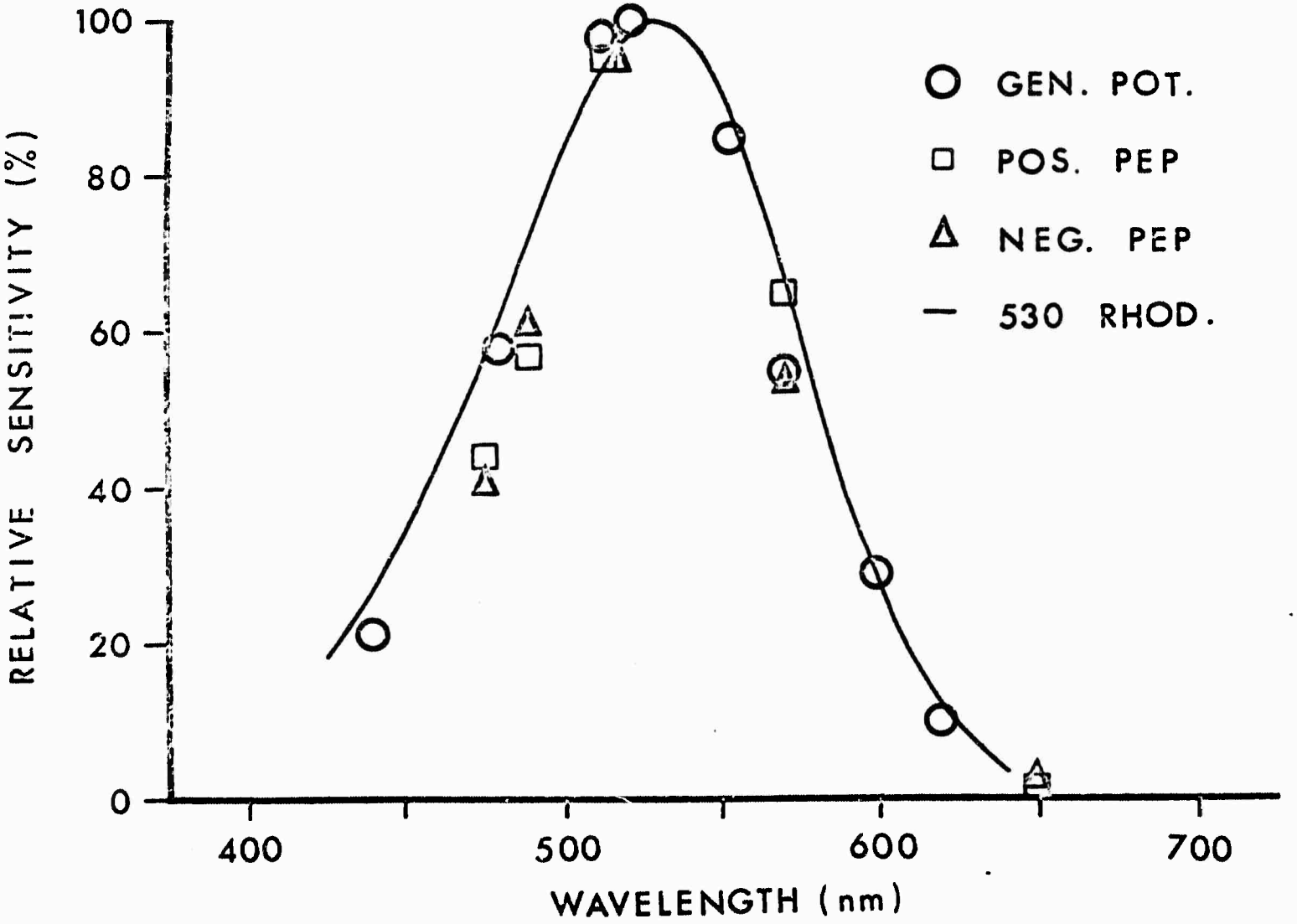
RELATIVE SENSITIVITY (%)
100
80
60
40
20
0
400
500
600
700
WAVELENGTH (nm)
GEN. POT.
POS. PEP
NEG. PEP
530 RHOD.

Motional Narrowing in Hydrogen Raman Scattering

J. R. Murray and A. Javan

This report describes the results of a high resolution study of the motional narrowing effect (the decrease in the normal Doppler linewidth when the mean free path becomes comparable to the wavelength of the emitted radiation (1 - 5)) in spontaneous Raman scattering in the Q(1) line of the 1-0 vibrational band of the hydrogen molecule. An argon ion laser is used as the exciting source, and the linewidth analysis is done with a Fabry-Perot interferometer.

We have reported qualitative preliminary observations of this effect previously (6). Motional narrowing was first seen in hydrogen by Rank and Wiggins in infrared absorption spectra (7). Narrowing has also been seen in stimulated Raman scattering in hydrogen (8). Cooper, May, et al. have obtained similar high resolution results for the rotational Raman lines of hydrogen. (9)

The argon ion laser operates at 4880Å and is a hollow cathode design with segmented graphite discharge tube (10). The laser is operated in a four mirror Michelson type cavity (11) to reduce the number of simultaneously oscillating modes, and has a linewidth of about 0.0085 cm^{-1}. (The linewidth under similar conditions in a two mirror cavity is about 0.1 cm^{-1}.) The center of this line is locked to an external Fabry-Perot reference to reduce frequency drifts, which otherwise are a severe limitation. The output power is about 50 milliwatts.

The laser beam enters a scattering cell which is a quartz capillary of 0.5 mm. inner diameter and 30 cm length. Reflection at grazing incidence from the walls of this capillary propagates the light scattered in

a small cone in the forward (parallel to the laser beam) and backward (anti-parallel) directions to the ends of the cell, where it is collimated by a lens and enters a pressure scanned Fabry-Perot interferometer of 0.79 cm^{-1} interorder spacing. The output of the Fabry-Perot is detected by an ITT FW-130 photomultiplier with pulse counting electronics and displayed on a chart recorder. Recordings are made at a temperature of 25°C. over a density range of 2 to 100 Amagat. Sample recordings exhibiting the line narrowing effect are shown in Figure 1. The dependence of the Q(1) line-width on density is shown in Figure 2. The instrumental linewidth (0.031 cm^{-1}) has been subtracted from each point.[1]

At high densities, ignoring pressure broadening effects, all models of the motional narrowing predict that the normal Gaussian Doppler profile will become a Lorentzian lineshape with full width at half maximum $\frac{D_0 k^2}{\pi d}$, where D_0 is the self-diffusion constant, k is the wave vector of the incident photon minus the wave vector of the emitted photon, and d is the density in Amagat units (density/density at 1 atm. pressure and 0°C). If pressure broadening is present and is not correlated with the motional narrowing (2-5), the resulting lineshape will be a Lorentzian of width $\frac{D_0 k^2}{\pi d} + ad$, where a is the pressure broadening coefficient, and is determined from the forward scattering data to be $1.68 \pm .07 \times 10^{-3}$ cm^{-1}/Amagat, which is in fair agreement with the calculations of Van Kranedonk (12) and the measurement at higher densities by May, et al. (13).

The solid line for the backward scattering in Figure 2 gives a fit to this simple diffusion model. The dotted line gives the behavior of a "hard collision" model (3, 4) in the region where it diverges from the simple diffusion model. This model assumed that the velocity of a molecule after a collision

has a Maxwell-Boltzmann distribution and is unrelated to its velocity before the collision. The diffusion constant D_o has been chosen for a best fit to this model, and is $1.35 \pm .10$ cm^2 Amagat/sec. A gas kinetic measurement of D_o (14), expressed in our units, and corrected for temperature, gives $D_o = 1.361 \pm .004$ cm^2 Amagat/sec. As a measure of fit of the experimental data to these models, the mean deviation of the experimental points from the simple diffusion model above 12 Amagat is (all in units of 10^{-3} cm^{-1}) + 0.9 and the root mean square deviation is ±3. For the hard collision model below 12 Amagat the mean deviation is +0.07 and the rms deviation ± 7.5. Noise in the points above 12 Amagat is primarily laser flicker. Statistical noise is important below 12 Amagat.

The dashed line gives the behavior of a Brownian motion or "soft collision" model (2, 4) for the same region and with the same value of D_o. This model assumes a small velocity change in a single collision. If D_o is chosen 10% lower for a best fit to the Brownian motion model, the mean deviation below 12 Amagat is -5 and the rms deviation ±10. Above 12 Amagat the mean deviation is +3 and the rms deviation is ±4. This is a noticeably worse fit than for the hard collision model, and indicates that the hard collision model is a better approximation for hydrogen.

We are presently extending these measurements to other lines in hydrogen and deuterium.

We would like to acknowledge very helpful discussions with Professor A.D. May.

REFERENCES

1. R. H. Dicke, Phys. Rev. 89, 472 (1953).
2. L. Galatry, Phys Rev. 122, 1218 (1961).
3. M. Nelkin and A. Ghatak, Phys. Rev. 135, A4 (1964).
4. S. G. Rautian and I. I. Sobelmann, Usp. Fiz. Nauk. 90, 209 (1966).
5. J. I. Gersten and H. M. Foley, J. Opt. Soc. Am. 58, 933 (1968).
6. J. Murray and A. Javan. Bull. Am. Phys. Soc. 12, 113 (1967).
7. D. H. Rank and T. A. Wiggins, J. Chem. Phys. 39, 1348 (1963).
8. P. Lallemand, P. Simova, and G. Bret, Phys. Rev. Lett, 17, 1239 (1966).
9. V. G. Cooper, A. D. May, E. H. Hara, and H. F. P. Knapp, Can. J. Phys. 46, 2019 (1968).
10. D. A. Huchital and J. D. Rigden, IEEE J. Quant. Elect. 3, 378 (1967).
11. P. W. Smith, IEEE J. Quant. Elect. 1, 343 (1965).
12. J. Van Kranedonk, Can. J. Phys. 41, 433 (1963).
13. A. D. May, V. Degen, J. C. Stryland, and H. L. Welsh, Can. J. Phys. 39, 1769 (1961).
14. P. Harteck and H. W. Schmidt, Z. Physik. Chem., Abt. B, 21, 447 (1933).

FIGURE CAPTIONS

Fig. 1: Sample chart recordings of the Q(1) Raman line of hydrogen, showing the dependence of linewidth on pressure. The small peak to the right is the Q(0) line in another order of the interferometer. The scanning speed was 0.025 cm^{-1}/min and the time constant 10 sec.

Fig. 2: Linewidth (full width at half maximum) of the Q(1) Raman line of hydrogen for forward and backward scattering. The Doppler broadening is destroyed as the density increases, and pressure broadening then becomes dominant. The instrumental linewidth has been subtracted. The theoretical fits are explained in the text.

FOOTNOTES

1. The line shape should be Lorentzian, and fits a Lorentzian to within the error of the experiment, above 12 Amagat in the backward direction and 2.5 Amagat in the forward direction, so that the Lorentzian instrumental width may be simply subtracted. Below 12 Amagat the lineshape should go smoothly from a Lorentzian to a Gaussian at zero density, but our noise at these low densities is too severe to get a detailed line shape. We have used a best Lorentzian fit to extract the linewidth.

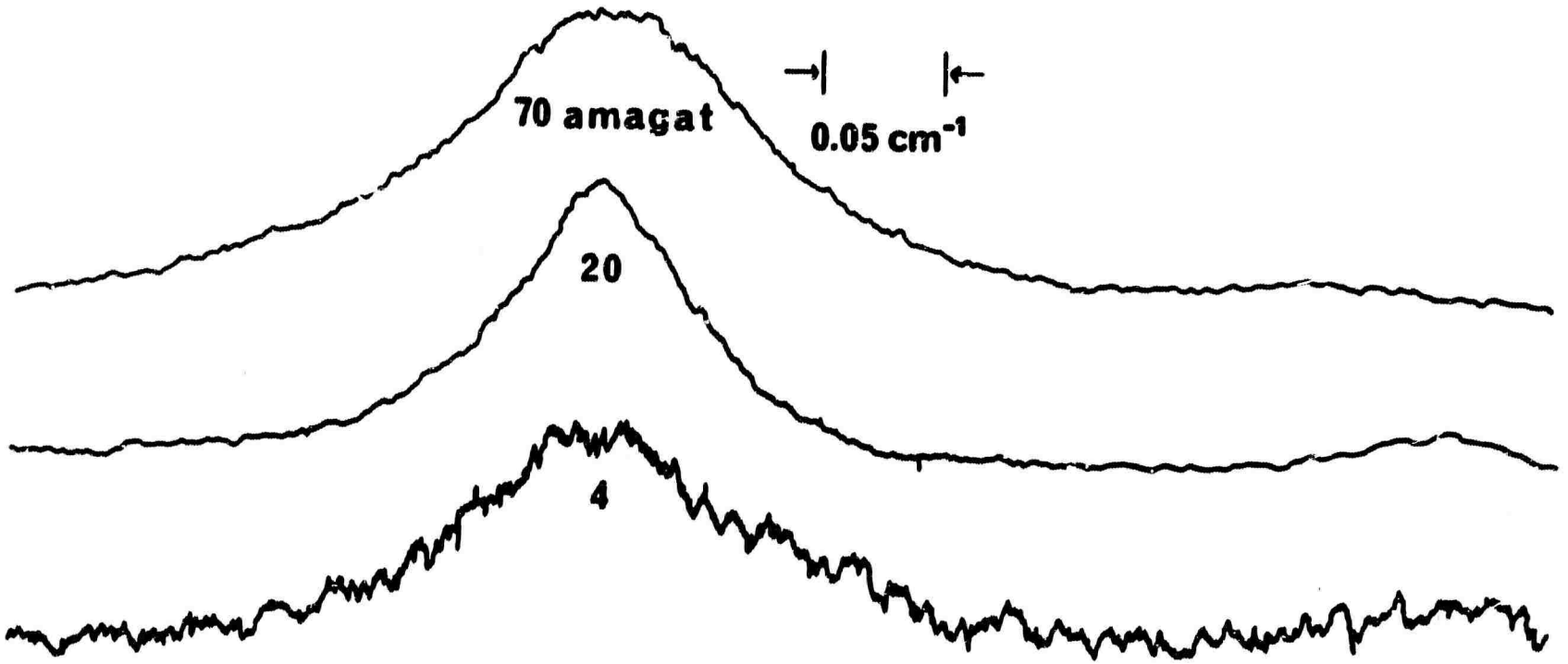
70 amagat
0.05 cm^{-1}
20
4

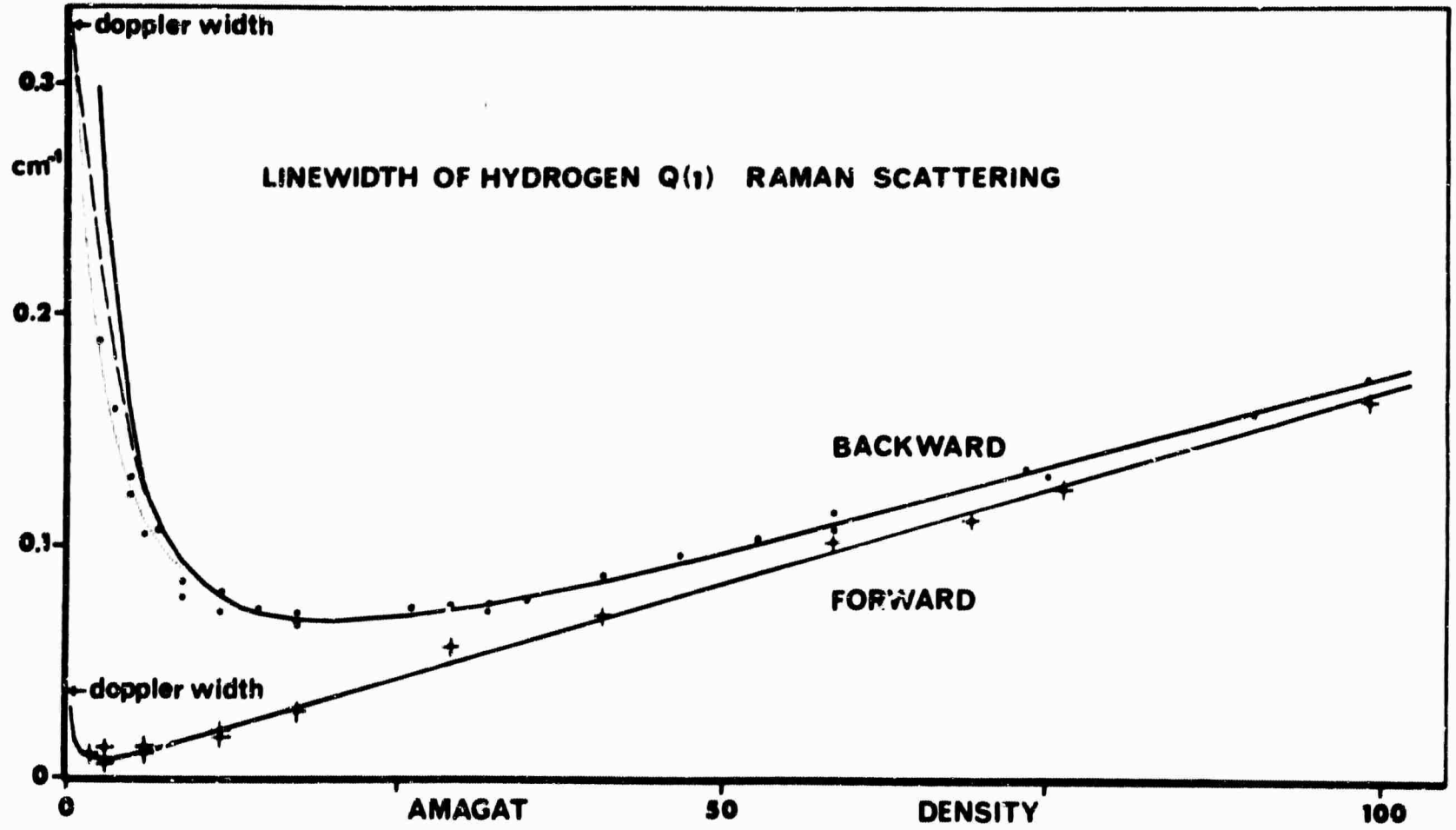
doppler width
0.3
cm⁻¹
LINEWIDTH OF HYDROGEN Q(1) RAMAN SCATTERING
0.2
BACKWARD
0.1
FORWARD
doppler width
0
0
AMAGAT
50
DENSITY
100

Frequency Spectrum of Spontaneous and Stimulated Line Narrowing Effects Induced by Laser Radiation*

M. S. Feld and A. Javan

In an earlier publication,[1] a laser-induced line narrowing effect was utilized in a precise determination of isotope shifts in two Ne transitions. A recent paper[2] also reports observation of this effect and its application in studying some linewidth parameters in Ne. These experiments study fluorescence arising from the lower level of a Doppler-broadened laser transition to a third level. [See Fig. 1(a).] Viewed along the laser axis, the broad fluorescence line shape is dramatically influenced by the laser field. For a standing-wave field detuned from its atomic center frequency, the laser-induced change signals appear as resonant increases in intensity over two narrow intervals symmetrically located on opposite sides of the fluorescence center frequency. The fluorescence from the upper laser level [Fig. 1(c)], similarly viewed, would exhibit narrow resonant decreases in its overall emission profile.

The overall features of this effect may be described by noting that the standing-wave laser field selectively interacts with atoms whose velocities Doppler-shift one of its travelling-wave components into resonance; this produces changes in the laser level populations--an increase in the lower level population and a decrease in the upper level population--over two narrow intervals symmetrically located about the center of the velocity distribution. A recent letter[3] has analyzed the line-shape details

for the cascade case [Fig. 1(a)] in terms of two-quantum transitions from level 2 to level 1, and predicts differing widths for the two laser-induced change signals. A similar line shape asymmetry, described below, would appear in the change signals from the upper laser level [Fig. 1(c)]. Note that in the latter case, however, the $0 \rightarrow 1$ emission act is an inherently single-quantum event, requiring another description. The summary of a different treatment[4] based on the density matrix formalism has described the spontaneous emission profile in both cases. Lineshape behavior of similar origins has been encountered in the microwave region in experiments involving the interaction of two monochromatic, classical fields with a three-level system.[5,6] These considerations may be readily extended to the present case by including the Doppler effect, and noting that the spontaneous emission spectrum from either laser level [level 0 of Figs. 1(a) and 1(c)] follows the emission line shape stimulated by a weak monchromatic field tuned through that resonance when the population of level 1 is ignored. In fact, recent experiments have studied the response of a Doppler-broadened three-level system coupled to two classical fields. The line-shape theory describing these experiments is directly applicable to important special cases of the effect observed in spontaneous emission. This letter has three intimately related objectives: The first is to point out the direct relevence of the detailed analyses of Refs. 7 and 8 to this problem; these also predict that one of the laser-induced resonances will be narrower than the other. Secondly, we emphasize that experiments based on stimulated versions of this effect demonstrate the different characteristics of the two laser-induced resonances. Thirdly, this letter generalizes the theory in several ways, including important power-broadening effects.

The analysis of Ref. 7 describes the third-order interaction of two monochromatic fields with the folded Doppler-broadened system of Fig. 1(b) in which

levels 1 and 2 are assumed to be closely spaced. Note that the analysis of a cascade system [Fig. 1(a)] in which the middle level lies about halfway between the other two levels follows identically. For purposes of illustration, let us assume that both transitions exhibit gain. Consider a strong standing-wave laser field $E_2(\Omega_2)$ detuned by an amount $|\Delta_2| > \gamma_{21} + \frac{1}{2}\gamma_0$ from ω_2, the peak of the 2-0 Doppler response [Fig. 1(b)]; here, $\gamma_{ij} = \frac{1}{2}(\gamma_i + \gamma_j)$, with γ_j the natural decay rate of level j. As a weak monchromatic field $E_1(\Omega_1)$ is tuned through the 1-0 transition, it is shown that the broad Doppler gain profile is considerable modified by the presence of E_2. The resulting line shape is obtained from Eqs. (33d) and (33e)[9] of Ref. 7:

$$P(\Omega_1) = G(\Omega_1)\left[1 + \xi E_2^{o2}\,\mathrm{Im}\left\{\frac{1}{(\Delta_2+\Delta_1) + i(\gamma_{21}+\gamma_0)} + \frac{1}{(\Delta_2-\Delta_1) + i\gamma_{21}}\right\}\right], \quad (1)$$

$\omega_1 \approx \omega_2$,

in which $\Delta_j = \Omega_j - \omega_j$, ω_j = atomic center frequency of j-0 transition, and Ω_j and E_j^o are frequency and amplitude of $E_j(\Omega_j)$, respectively; $G(\Omega_1)$ is the linear Doppler response, a slowly varying function of Ω_1, and ξ is a constant factor. For Ω_2 above ω_2, (1) predicts narrow Lorentzian responses of widths $\Gamma_B = \gamma_1 + \gamma_2 + 2\gamma_0$ below ω_1 and $\Gamma_N = \gamma_1 + \gamma_2$ above ω_1, the latter being narrower by $2\gamma_0$ and independent of γ_0. In subsequent discussion we shall refer to the "broad" (Γ_B) and "narrow" (Γ_N) resonances, respectively.

The narrow resonance, Γ_N, predicted by (1) has been observed and fully verified[10] for $\Gamma_N \ll \Gamma_B$. In these experiments levels 1 and 2 are tunable Zeeman components of an upper laser level connected to a common lower level, 0. The monochromatic fields are two oscillating laser modes of fixed frequencies determined by the cavity length. The effect is observed as sharp decreases in the laser output as the 2, 1 level splitting is magnetically tuned. These methods, however, have not been applied to the observation of Γ_B, which requires absolute frequency control as in Lamb-dip

experiments. (See Ref. 7.)

We report here an extraordinary manifestation of the broad resonance, observed in high-resolution studies of the $3p\,^3P_{0,2,1}$-$3s\,^3S_1$ atomic oxygen fine-structure laser oscillations at 8446 Å. The relevant fine-structure components of this system consist of two resolved and closely spaced Doppler-broadened transitions forming folded three-level systems of the type shown in Fig. 1(b). For reasons unrelated to the present discussion, [11] (i) the central portion of each of the fine-structure gain profiles is entirely depleted and appreciable gain exists only on the wings; and (ii) laser action most readily occurs on the high-frequency side of the strongest (2-0) fine-structure component. For each laser mode oscillating on the 2-0 transition, two Lorentzian holes of enormously different widths selectively deplete the 1-0 Doppler gain profile; the low-frequency hole, of width $2\gamma_0+\gamma_1+\gamma_2=130$ MHz, is about 15 times broader than the high-frequency hole, of width $\gamma_1+\gamma_2=9$ MHz. [13] Because of multimoding on the 2-0 transition, multiple hole pairs are burnt into the 1-0 transition. The broad low-frequency holes overlap, completely suppressing laser action below the 1-0 line center, and oscillation can occur between the narrow, nonoverlapping holes above the center frequency. The 8446 Å spontaneous emission and laser output have been studied photographically with a high-resolution Fabry-Perot interferometer with free spectral range of 0.8 cm^{-1} under a wide range of conditions. The laser oscillations were obtained in argon-oxygen and neon-oxygen mixtures, [14] using a 3-meter cavity with 50 MHz mode spacing. The operating pressure was kept below 1 torr to minimize pressure broadening effects. To establish the frequency shifts, Fabry-Perot images of the laser oscillations and the spontaneous emission were superimposed upon the same glass plate emulsion. In absence of laser oscillation, the spontaneous-emission analysis shows, in order of increasing frequency: a well-resolved fine-structure

component (1-0) with a completely symmetrical profile, and the strongest fine-structure component (2-0), overlapped on the high-frequency wing by the third (weak) fine-structure component. Close to threshold, laser oscillation first occurs on the high-frequency wing of the 2-0 component, where maximum gain occurs, as explained in Footnote 11 (ii). Further above threshold the 1-0 transition also breaks into oscillation. Despite the observed symmetry of the 1-0 profile, this concurrent oscillation occurs above the 1-0 center frequency, an effect which must follow from the depletion of gain over the entire low-frequency wing, as described above. (It must also be pointed out that in the observations reported here the 1-0 oscillation was at all times close to threshold and considerably weaker than the 2-0 oscillation.[15])

Reference 7 treats the field interactions up to third order. We now outline a different approach,[8] formulated in terms of single- and double-quantum transitions, which includes power-broadening effects due to a strong laser field. The latter are of considerable interest: on the theoretical side, it is important to inspect whether or not the strikingly simple line-shape behavior is merely characteristic of a third-order culation; on the experimental side, it is important to know the influence of power broadening on the observed line shape. Consider the cascade system of Fig. 1(a). [The final result will be written in a form also valid for emission from the upper laser level, Fig. 1(c).] It is desired to calculate the 0-1 emission spectrum stimulated by the weak travelling-wave field $E_1(\Omega_1)$ in the presence of the strong standing-wave field $E_2(\Omega_2)$ coupled to the 2-0 transition. Specifically standing-wave effects are avoided by taking Ω_2 detuned ($|\Delta_2| > \gamma_{20}$); then oppositely propagating travelling-wave components of E_2 do not couple, and the interaction consists of these components independently coupled with E_1.

Consider an ensemble of atoms moving with given axial velocity v,

the $+z$ axis being defined by the propagation direction of the travelling-wave field E_1. In the atoms' rest frame the incident fields appear Doppler-shifted to frequencies $\Omega_1' = \Omega_1 (1 - \frac{v}{c})$ and $\Omega_2' = \Omega_2 (1 - \epsilon \frac{v}{c})$ in which $\epsilon = \pm 1$ indicates the travelling-wave component of E_2 propagating along the $\pm z$ direction, respectively. We now require a solution in the atoms' rest frame in which the three-level system is coupled to one of the travelling-wave components of the strong field E_2 at frequency $\Omega_2' \sim \omega_2$ and to the weak travelling-wave field E_1 at frequency $\Omega_1' \sim \omega_1$. The resonant interaction of two monochromatic fields with a three-level system was treated in Ref. 5 for the case of γ_j all equal. The perturbation method consisted of first obtaining a closed form solution to the Schrödinger equation for $E_1^o = 0$ and E_2^o arbitrary; and then using this result to generate a solution valid to first order in E_1^o. When the method is extended to the case of arbitrary γ_j,[16] the emitted power induced by E_1 at Ω_1' is:

$$8\hbar\Omega_1' |\beta_1|^2 \operatorname{Im}\left[n_2 |\beta_2|^2 \frac{(L_2 - 2\frac{\gamma_{20}}{\gamma_0} R)}{AB} + n_1 \frac{R}{B} - n_0 \left\{ \frac{R}{B} + |\beta_2|^2 \frac{(L_2 - 2\frac{\gamma_{20}}{\gamma_0} R)}{AB} \right\} \right]. \quad (2)$$

Here, $A = |L_2|^2 + \frac{4\gamma_{20}^2}{\gamma_0\gamma_2} |\beta_2|^2$ and $B = -RL_1^* + |\beta_2|^2$, with $L_j = (\Omega_j' - \omega_j) + i\gamma_{j0}$, $R = [(\Omega_1' + \Omega_2') - (\omega_1 + \omega_2)] - i\gamma_{21}$, $|\beta_j| = |\mu_{j0} E_j^o / 4\hbar|$, and μ_{j0} is the electric-dipole matrix element connecting levels j and 0; n_j is the number of background atoms with velocity v in level j, i.e. the population in absence of the strong laser field. In Eq. (2) the n_2 coefficient is obtained from the $2 \rightarrow 1$ transition rate due to double-quantum emission at Ω_1' and Ω_2'; then n_0 coefficient, in contrast, is obtained from the single-quantum emission rate, arising from $0 \rightarrow 1$ transitions as modified by the presence of E_2; the n_1 coefficient results from the reverse processes, namely, double-quantum $1 \rightarrow 2$ transitions and single-quantum $1 \rightarrow 0$

transitions.[17] (See Ref. 5) As a check of the detailed algebra, Eq. (2) has also been obtained in an independent calculation using the ensemble-averaged density matrix to estimate the induced polarization at Ω_1', an approach equivalent to the one presented here.[8]

It is important to note that (2) is entirely valid for the case in which the γ_j's are interpreted as decay rates arising from hard collisions. The detailed features of the line shape predicted[5] by (2) for equal γ_j have been fully verified in the microwave region where Doppler effect is negligible and the linewidths are entirely due to collision effects.[6]

The complete emission spectrum is obtained by averaging (2) over the atomic velocity distribution for $\epsilon = +1$ and for $\epsilon = -1$. In the fully Doppler-broadened limit $\gamma/D \ll 1$ ($\gamma \sim \gamma_{ij}$ and D= Doppler width), and for $\omega_1 \geq \omega_2$,

$$P(\Omega_1) = G(\Omega_1)\left[1 + \frac{N_0 - N_2}{N_0 - N_1}\,\xi'\,E_2^{o2}\,\mathrm{Im}\left\{\frac{1}{(\Delta_1 + \sigma\frac{\omega_1}{\omega_2}\Delta_2) + i\frac{\Gamma_B}{2}} + \frac{1}{(\Delta_1 - \sigma\frac{\omega_1}{\omega_2}\Delta_2) + i\frac{\Gamma_N}{2}}\right\}\right], \quad (3)$$

in which $\frac{1}{2}\Gamma_B = \gamma_{10} + \frac{\omega_1}{\omega_2}\gamma_{20}Q + \frac{\gamma_0}{2}(Q-1)$ and $\frac{1}{2}\Gamma_N = \gamma_{10} + \frac{\omega_1}{\omega_2}\gamma_{20}Q - \frac{\gamma_0}{2}(Q+1)$; N_j is the total background population of level j, ξ' is a proportionality factor > 0, $Q^2 = 1 + \frac{4|\beta_2|^2}{\gamma_0\gamma_2}$, and $G(\Omega_1) \propto (N_0 - N_1)E_1^{o2}$ is the power emitted at Ω_1 by the Doppler-broadened 0-1 transition induced by E_1 in the absence of the laser field. Equation (3) shows the power broadening influence of the laser field, which enters in a remarkably simple way. Equation (3) has been written in a form valid for both cascade ($\sigma = -1$) and folded ($\sigma = +1$) cases, Figs. 1(a) and 1(c).[18]

As pointed out above and explained in Ref. 18, the spontaneous emission spectrum from the upper or lower laser levels, as viewed along the laser axis, is also given by Eq. (3) when N_1 is set equal to 0 and $G(\Omega_1)$ is interpreted as the usual Doppler-broadened spontaneous emission spectrum for $E_2 = 0$.

The discussions of Ref. 3 are consistent with weak-field limit of our treatment as it applies to spontaneous emission for the special case of $N_0 = 0$. Note, for instance, that for $|\beta_2| \ll \gamma$ and in the limit of $\gamma_{21} \to 0$, the frequency dependence of the $2 \to 1$ transition rate, obtained from the n_2 coefficient of our Eq. (2),

would involve a δ-function, becoming $\delta(\Omega_1' + \Omega_2' - \omega_1 - \omega_2)\,|L_2|^{-2}$; the $\gamma_{21} = 0$ discussion of Ref. 3 is equivalent to averaging this distribution over velocities.

To emphasize the significance of the role played by N_0, the background atoms in level 0, consider a cascade system in which only level 0 is populated (i.e. $N_1 = N_2 = 0$). Then in the rest frame of an atom, an applied laser field at Ω_2' will diminish the transition rate at Ω_1', leading to two holes of width Γ_B and Γ_N superimposed upon the emission profile. [See Eq. (3).] As discussed earlier, a $0 \rightarrow 1$ transition is an inherently single-quantum event [5] and may not be described in terms of a double-quantum process as in a $2 \rightarrow 1$ transition.

As pointed out above, in the oxygen[10,12] and xenon[10] experiments Γ_B and Γ_N differ enormously. In the Ne spontaneous emission experiments reported ir Refs. 1 and 2, however, they are expected to differ by only about 30%. The observation of this difference would require high finesse Fabry-Perot analysis and good laser stability and has not yet been achieved.

In averaging Eq. (2) for the case of finite γ_{21} a number of cancellations occur in the fully Doppler-broadened limit ($\gamma/D \ll 1$), leading to a particularly simple expression. It is important to point out that such cancellations do not occur in higher orders of γ/D. For instance, the complete cancellation of γ_0 in Γ_N, which occurs in the case of $\omega_1/\omega_2 \approx 1$, will not occur in the next order of γ/D.

A paper including complete algebraic details and additional discussions is being submitted for publication.[8]

REFERENCES

1. R. H. Cordover, P. A. Bonczyk, and A. Javan, Phys. Rev. Letters 18 730, 1104 (E) (1967).

2. W. G. Schweitzer, Jr., M. M. Birky, and J. A. White, JOSA 57, 1226 (1967).

3. H.K. Holt, Phys. Rev. Letters 19, 1275 (1967).

4. M.S. Feld and A. Javan, Bull. Am. Phys. Soc. 12, 1053 (1967).

5. A. Javan, Phys. Rev. 107, 1579 (1957).

6. T. Yajima, J. Phys. Soc. Japan 16, 1709 (1961); A.P. Cox, G.W. Flynn, and E.B. Wilson, J. Chem. Phys. 42, 3094 (1965).

7. H.R. Schlossberg and A. Javan, Phys. Rev. 150, 267 (1966).

8. M.S. Feld, Ph.D. Thesis, M.I T., 1967; M.S. Feld and A. Javan, "Laser-Induced Line Narrowing Effects in Coupled Doppler-Broadened Transitions", Phys. Rev., to be published.

9. There are several relevant misprints in Eq. (33): in line (33e), E_1E_2 should read $E_1E_2^2$; line (33d) should read:
$+ (|\mu_{12}\mu_{31}|^2/\gamma_1)(N_3 - N_1)\frac{1}{2}E_1E_2^2 \; [\gamma - i(\omega_B - \nu_B)]^{-1}$.

10. H.R. Schlossberg and A. Javan, Phys. Rev. Letters 17, 1242 (1966); G.W. Flynn M.S. Feld and B.J. Feldman, Bull. Am. Phys. Soc 12, 669 (1967).

11. For explanation of (i), see Refs. 8 and 12; (ii) is merely due to the presence of the weak fine-structure component with gain ($^3P_0 - ^3S_1$), which overlaps the high-frequency wing of the 2-0 transition ($^2P_2 - ^3S_1$). The 1-0 transition ($^3P_1 - ^3S_1$), however, is completely symmetrical and free of overlap.

12. M S. Feld, B.J. Feldman and A. Javan, Bull. Am. Phys. Soc. 12 669 (1967); "Frequency Shifts of the Fine Structure Oscillations of the 8446 Å Atomic Oxygen Laser", Phys. Rev., to be published.

13. For Oxygen linewidths, see: W.L. Wiese, M W. Smith and B.M. Glennon, Atomic Transition Probabilities, Vol. 1, U.S. Department of Commerce, National Bureau of Standards, Wash. D.C.

14. W.R Bennett, Jr., W.L. Faust, R.A. McFarlane, and C.K.N. Patel, Phys. Rev. Letters 8, 470 (1962).

15. A study of the intensity of the 1-0 laser oscillation as a function of cavity length would be of interest.

16. In this case the time-dependent wave-function Ψ is obtained from a three-level Schrödinger equation to which radiative decay terms have been added. For $\Psi = \sum_{j=0}^{2} c_j e^{-iW_j t} u_j$, with u_j the eigenfunction of level j of energy $\hbar W_j$, the coupled equations are: $\dot{c}_i = \sum_j (a_{ij} - \frac{1}{2}\gamma_j \delta_{ij}) c_j$ in which $a_{ij} = -\frac{\mu_{ij} E(t)}{i\hbar} e^{i(W_i - W_j)t}$, and $E(t)$ is the sum of the two travelling-wave fields as seen in the atoms' rest frame.

17. As an example, for an atom in level 0 at initial time t_0, $|c_j(t=t_0, t_0)|^2 = \delta_{j0}$, and the $0 \rightarrow 1$ transition rate at a later time t is $\gamma_1 |c_1(t, t_0)|^2$. (See preceeding footnote.) Thus, the total stimulated power emitted by background atoms in level 0 is $\hbar \Omega_1' n_0 \gamma_0 \gamma_1 \int_{-\infty}^{t} |c_1(t, t_0)|^2 \, dt_0$.

18. In extending Eq. (2) to the spontaneous emission case, the population of level 1, n_1, should be set equal to 0 and the energy density of the weak probe field, $E_1^{o\,2}/8\pi$, should be replaced by $(\hbar\Omega_1'^3 / 8\pi^3 c^3) d\Omega_1' dS$, where frequency interval $d\Omega_1' \ll \gamma$ and dS is a small solid angle in the forward direction ($\pm z$ - axis); E_2, the laser field, remains in its classical monochromatic form. Similar remarks apply to Eq. (3); note, in particular, that $G(\Omega_1)$ becomes the usual Doppler-broadened spectrum of the power emitted spontaneously into $d\Omega_1 \, dS$ with given polarization.

FIGURE CAPTIONS: The figure caption is contained in the figure.

DOCUMENT CONTROL DATA - R & D

Security classification of title, body of abstract and indexing annotation must be entered when the overall report is classified

1 ORIGINATING ACTIVITY (Corporate author)
Massachusetts Institute of Technology
Cambridge, Mass. 02139

2a. REPORT SECURITY CLASSIFICATION
unclassified

2b GROUP

3 REPORT TITLE
"Study of Various Aspects of Raman Scattering Using Gas Lasers"

4 DESCRIPTIVE NOTES (Type of report and inclusive dates)
Final report 3/1/67 through 7/31/68

5 AUTHOR(S) (First name, middle initial, last name)
Professor Ali Javan; principal investigator

6 REPORT DATE	7a TOTAL NO OF PAGES	7b NO OF REFS
approx. issue date	110	97

8a CONTRACT OR GRANT NO	9a ORIGINATOR'S REPORT NUMBER(S)
Nonr 3963(22) Mod. = 1 and 2	Final report
b PROJECT NO NR 014-209/7-17-67	
c	9b OTHER REPORT NO(S) (Any other numbers that may be assigned this report)
d ARPA order = 306	

10 DISTRIBUTION STATEMENT
Distribution of this document is unlimited.

11 SUPPLEMENTARY NOTES	12 SPONSORING MILITARY ACTIVITY
	Office of Naval Research Advanced Research Projects Agency ARPA order = 306

13 ABSTRACT

Several aspects of non-linear interaction of laser radiation with atomic resonances are theoretically explored. These effects are manifested through multiple quanta processes and yield novel types of line narrowing effects; these effects are observed in great detail and applied in precision studies of the structure the structure of atomic resonances. Motional linewidth narrowing in spontaneous Raman scattering is observed using an argon laser.

14 KEY WORDS	LINK A		LINK B		LINK C	
	ROLE	WT	ROLE	WT	ROLE	WT
Raman effect						
multiple quanta processes						
line-narrowing						